ISET JOURNAL OF EARTHQUAKE TECHNOLOGY

Vol. 49 No. 3-4 September-December 2012

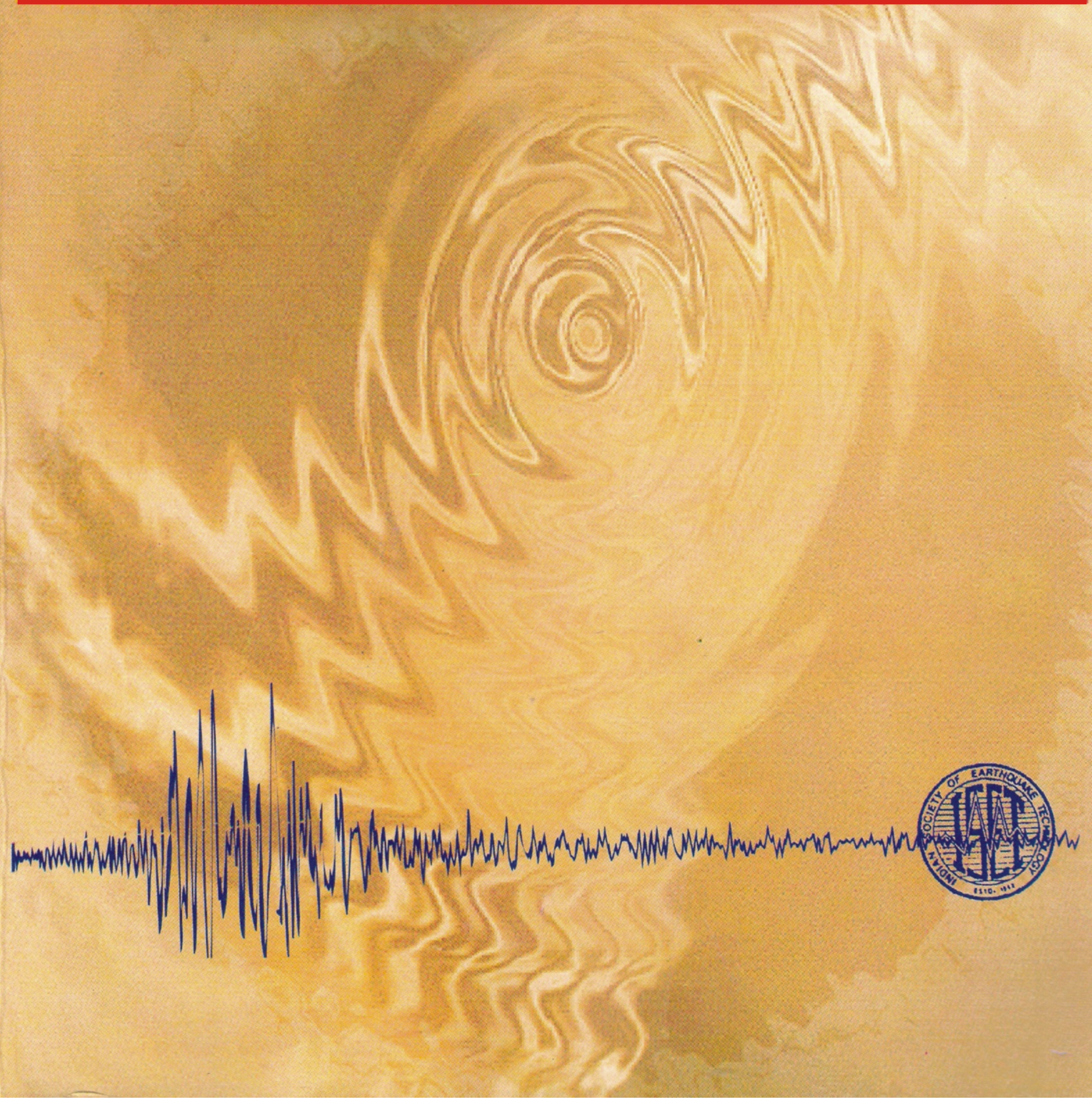

INDIAN SOCIETY OF EARTHQUAKE TECHNOLOGY
AIMS AND OBJECTIVES

i. To provide necessary forum for scientists and engineers of various specializations to come together and exchange ideas on the problems of earthquake technology.
ii. To disseminate knowledge in the field of earthquake technology dealing with seismological and engineering aspects.
iii. To promote research and development work in the field of earthquake technology.

ISET JOURNAL OF EARTHQUAKE TECHNOLOGY

The ISET Journal of Earthquake Technology is published quarterly in the months of March, June, September & December by the Indian Society of Earthquake Technology (ISET). It was first published in 1964 under the name of Bulletin of the Indian Society of Earthquake Technology and is renamed as ISET Journal of Earthquake Technology from the year 1998.

MEMBERSHIP AND SUBSCRIPTION

The membership of the Society is open to all Individuals and Institutions connected with or interested in any scientific, engineering and other aspects of Earthquake Technology.

For ISET members, subscription to the ISET Journal is included in the membership fee. The subscriptions are by annual volume only. The subscription rate for non-members is Rs.2000/- (US$ 200) per volume. Individuals and institutions may apply for membership on prescribed form obtainable from the Secretary on request. Back numbers of the previous Bulletins and the Journals, as in stock, can be obtained from the Secretary on full subscription payment. The rates per issue are given below:

For Non-Members	Rs. 750/- (US$ 50 by air mail)
For Special Issue	Rs. 1500/- (US$ 80 by air mail)

COMMUNICATION

Communications regarding change of address, subscription renewals, missed numbers, membership and Society publications should be addressed to the Secretary, Indian Society of Earthquake Technology, Department of Earthquake Engineering Building, IIT Roorkee, Roorkee-247 667, Uttarakhand, India, E-mail: ***office@iset.org.in; iset@iitr.ernet.in***

COPYRIGHT

MANUSCRIPT

Manuscript offered for publication in the ISET Journal should be submitted to the Editor. Members may also send news items, memoirs, book reviews and news about the activities of the ISET Local Chapters to the Co-Editor for publication in the ISET News Letter. Authors are given 25 reprints free of charge. Request for additional reprints, if desired, must be made immediately after acceptance of the paper is communicated to the authors. Reprints are supplied at the rate of Rs. 25/- (US$ 3) per reprint with a minimum charge of Rs. 500/- (US$ 75). The Society is not responsible for statements and opinions expressed by the authors in the Journal.

ISSN 0972-0405

ISET JOURNAL OF EARTHQUAKE TECHNOLOGY

Vol. 49	No. 3-4	September-December 2012

CONTENTS

Financial Assistance from DST, New Delhi for the Publication of ISET Journals for 2012–2013 is duly acknowledged.

ISET Journal of Earthquake Technology, Paper No. 521, Vol. 49, No. 3-4, Sept.-Dec. 2012, pp. 53–71

EFFECTIVE CONTROL OF EARTHQUAKE RESPONSE USING TUNED LIQUID DAMPERS

Mohan Murudi* and Pradipta Banerji**
*Department of Structural Engineering
Sardar Patel College of Engineering, Mumbai-400058
**Department of Civil Engineering
Indian Institute of Technology Bombay, Mumbai-400076

ABSTRACT

An earlier numerical study of a single-degree-of-freedom (SDOF) structure rigidly supporting a tuned liquid damper (TLD) and subjected to broad-band ground motions, has showed that a TLD has to be properly designed for effectively reducing the response of the structure. In this paper, a comprehensive study of the effects of various ground motion parameters on the ability of a TLD to reduce structural response for earthquake base motions is presented. It is shown that the frequency content and bandwidth of the ground motion do not significantly affect the effectiveness of the TLD. Since TLD is a nonlinear system, its effectiveness increases with an increase in the intensity of the ground motion. Furthermore, since TLD behaves as a viscous damper, it cannot reduce the response in the first few cycles of vibration. Therefore, TLD is more effective for the far-field ground motions, where the strong-motion phase and consequently the peak response of the structure occur after the first few cycles of vibration.

KEYWORDS: Earthquake Response, Structural Control, Tuned Liquid Damper, Energy Dissipation, Nonlinear Damping

INTRODUCTION

A variety of passive control devices have been developed to control the vibrations of civil engineering structures due to dynamic loads, such as those due to wind, earthquakes, etc. The passive energy dissipation systems encompass a range of materials and devices for enhancing damping, stiffness and strength and can be used both for natural hazard mitigation in new structures and for the rehabilitation of ageing or deficient structures. In recent years, serious efforts have been undertaken to develop the concept of energy dissipation or supplemental damping into a workable technology and a number of these devices have been used throughout the world.

Base isolation is one of the passive ways of controlling vibrations due to ground motions. The basic aim of base isolation is to shift the fundamental period of a structure away from the high-energy period of the ground motion, such that the structure is subjected to lower earthquake forces. A base isolation system causes a large displacement at the level of isolator, which needs to be accommodated or reduced by the supplemental means. The effectiveness of base isolation systems for controlling the seismic response of structures subjected to far-field ground motions has been well established.

In recent years, there has been a considerable interest in studying the response of base-isolated buildings under the recorded near-fault earthquake motions (Jangid and Kelly, 2001). These ground motions contain one or more displacement pulses with peak velocities of the order of 0.5 m/s and durations in the range of 1–3 s. Such pulses have a large impact on the isolation systems with periods in this range and lead to large isolator displacements.

Jangid and Kelly (2001) have studied the effectiveness of base isolation systems for near-fault motions. In their investigation, analytical studies of base-isolated structures were carried out. First, six pairs of near-fault motions oriented in directions parallel and normal to the fault were considered, and then the average of the response spectra of these earthquake records was obtained. This study has shown that, in addition to the pulse-type displacements, these motions contain significant energy at high frequencies and that the real and pseudo-velocity spectra are quite different. The second analysis modelled the response of a model of an isolated structure with a flexible superstructure to study the effect of isolation damping on the performance of different isolation systems under near-fault motions. The results have shown that there exists a value of isolation system damping for which the superstructure acceleration for a given structural system attains a minimum value under the near-fault motions. Therefore, although increasing the bearing damping beyond a certain value may decrease the bearing displacement, it may also transmit higher accelerations into the superstructure. Finally, the behaviour of four isolation systems subjected to the normal component of each of the near-fault motions was studied and it has been seen that EDF-type isolation systems may be the optimum choice for the design of isolated structures in near-fault locations.

Ye and Li (2009) have carried out a parametric study on the dynamic response of lead-rubber bearing (LRB) base-isolated structures under the near-fault pulse-like ground motions. Due to the limited number of real near-fault pulse-like records, for the convenience of the parametric study, artificially generated near-fault pulse-like ground motions were simulated by combining the real far-field ground motions with simple equivalent pulses that reflect the near-fault features. By using these artificially generated near-fault ground motions, different dynamic characteristics of LRB base-isolated structures under the near-fault pulse-like and far-field ground motions were studied. Moreover, the effects of different pulse types, near-fault ground motion parameters and dynamic properties of LRB isolation system on the maximum absolute acceleration of superstructure and maximum displacement at the isolation level were investigated. It has been concluded from this comprehensive study that the maximum absolute acceleration of superstructure and the maximum displacement at the isolation level of the LRB base-isolated structure subjected to near-fault pulse-like ground motions are much greater than those under the far-field ground motions. Further, the effective range of base isolation has been narrowed, and it has been seen that pulse type and pulse period have significant influences on the dynamic response of LRB base-isolated structures.

Another class of passive devices that are commonly used consists of tuned mass dampers (TMDs) (Den Hartog, 1956; Warburton, 1982; Villaverde, 1994). A TMD consists of a secondary mass with properly tuned spring and damping elements such that the dynamic characteristics of the structure are changed and a frequency-dependent hysteresis is provided to increase damping in the structure. It has been well established that TMD is effective in reducing the wind-excited structural vibrations. Kamrani-Moghaddam et al. (2006) have investigated the performance of TMDs in the response reduction of structures for near-field and far-field earthquakes. The 3-, 9- and 20-story structures designed for the SAC phase II project were used in this study. First, time-history analyses were performed to calculate the response of each structure to the Chi-Chi, Kocaeili and Landers near-field and far-field earthquake records. The same procedure was followed for the models with a TMD duly attached. The results have shown that the performance of TMD in the 3-story structure was better for the far-field excitations, while in the 20-story structure, the performance was better for the near-field excitations.

Pinelli et al. (2003) have studied and compared the feasibility and effectiveness of controlling the seismic vibrations of a structure through the installation of different combinations of TMDs. These include a single TMD tuned to one mode, multiple single TMDs controlling several modes (i.e., MTMDs), a battery of TMDs controlling one mode, also known as distributed tuned mass dampers (DTMDs), and several batteries controlling different modes, also known as multiple distributed tuned mass dampers (MDTMDs). The optimization criteria for each TMD combination were adopted from the literature, and modified as needed. Three public benchmark case studies were retrofitted with different combinations of TMDs and subjected to a series of earthquake ground motions with different durations and energy contents. The performance of each TMD scheme was evaluated based on the floor displacement and acceleration reduction as well as on the reduction of hysteretic energy dissipation in the structure. The influence on the performance of the TMDs of the nonlinear behavior of the structural members was also investigated. To evaluate the proposed control strategies under the benchmark evaluation study, two far-field and two near-field historical records were selected. From this study, the authors have concluded that under the far-field long-duration ground motions, both single-TMD and MTMD control methods can reduce the building response effectively. On comparing the results of the two methods, the MTMD control method has been found to give on average about 10% more acceleration reduction than the single-TMD control method. In the case of displacement reduction, both single-TMD and MTMD control methods have been found to perform similarly and larger mass ratios have resulted in bigger response reductions. However, the performance of both TMD and MTMD methods under the near-field earthquake motions has not been found to be significantly different.

More recently, Matta (2011) has investigated three classical techniques and tested two new variants for designing a TMD on an SDOF structure under 338 NF records from the PEER NGA database, including 156 records with the forward-directivity features. Percentile response reduction spectra were introduced to statistically assess the TMD performance, and TMD robustness was verified through the Monte Carlo simulations. The methodology was extended to a variety of MDOF bending-type and shear-type frames and a case-study building structure recently constructed in central Italy. It has been concluded that, if properly designed and sufficiently massive, TMDs are effective and robust even under the excitation of pulse-like ground motions. The two newly proposed design techniques have been shown to generally outperform the classical ones.

As discussed above, a base isolation system causes a large displacement at the level of isolator, especially when the system is subjected to the near-fault ground motions, and therefore this requires additional devices to control the isolator displacement. Taniguchi et al. (2008) have studied the effectiveness of TMD consisting of a mass-dashpot-spring subsystem that is attached to the isolated superstructure, analogous to a pendulum. Both the isolated superstructure and the TMD were modelled as linear single-degree-of-freedom oscillators. The optimal TMD parameters were determined by considering the response of the base-isolated structure, with and without the TMD, to a white-noise base acceleration time-history. Such an excitation is representative of the broad-band ground motions having a nearly constant intensity over a duration several times longer than the period of the base-isolated structure. It has been found that under such an excitation, a reduction of the order of 15–25% in the displacement demand of the base-isolated structure can be achieved by adding a TMD. Next, the responses of an example base-isolated structure with and without an optimally designed TMD to the selected suites of far- and near-field recorded accelerograms were determined. This study has shown that for the far-field ground motions, the effectiveness of TMD is more or less similar to that predicted by the white-noise model, whereas for the near-field ground motions, the effectiveness of TMD is of the order of 10% or less.

Tuned liquid dampers (TLDs) have been the subject of significant research over the past two decades. A TLD is essentially a tank which is attached to a structure to control its vibrations and whose size and water level are decided based on the structural requirements. Its appeal lies in its simplicity, cost-effectiveness and low maintenance requirements. It has already been implemented for controlling the wind-induced vibrations in structures (Tamura et al., 1995; Modi et al., 1995).

Studies have been carried out to study the effectiveness of TLDs for suppressing the response of structures to base excitations (Chaiseri et al., 1989; Sun et al., 1992; Yu et al., 1999). These studies were concentrated essentially on the harmonic base excitations. The authors have carried out a numerical study (Banerji et al., 2000) that has shown that TLDs, if properly designed, are effective in controlling the response of structures subjected to broad-band earthquake ground motions. The experimental studies by Banerji et al. (2010) have illustrated that a properly designed TLD is slightly more effective than the numerical predictions.

Sakai et al. (1989) have proposed another kind of liquid dampers, known as tuned liquid column dampers (TLCDs), which impart indirect damping to the primary structure through the oscillations of the liquid column in a U-shaped container. The energy dissipation in the water column results from the passage of the liquid through an orifice with inherent head-loss characteristics. The overall damping in a TLCD depends on the head-loss coefficient and the velocity of the oscillating liquid, and it is nonlinear due to the quadratic damping term. A simple macroscopic model of TLCD was also developed and verified through a series of experiments.

Yalla and Kareem (2000) have developed a new approach by using the TLCD theory and equivalent linearization scheme to compute the optimum head loss coefficient for a given level of wind or seismic excitation in a single step and without resorting to any iteration. The optimal damping coefficient and tuning ratio of a TLCD have been obtained by using a single-degree-of-freedom system under the white-noise excitation and a set of filtered white-noise excitations representing the wind and seismic loadings. The optimum values of damping have also been investigated for multiple TLCDs.

The overall damping in a TLCD depends on the head-loss coefficient and velocity of the oscillating liquid. The effectiveness of a TLCD depends on the optimum tuning and optimum damping coefficient. TLCDs have been studied significantly in the past and their behaviour is fairly well understood. The behaviour of a TLD is highly nonlinear and the energy dissipated by a TLD depends on the amount of sloshing rather than tuning. Therefore, the effectiveness of a TLD increases with an increase in the intensity of base motion. This behaviour needs to be studied further and hence the focus is on TLDs in this paper.

In this paper, a comprehensive study of the effectiveness of a TLD in controlling the earthquake response of a structure is presented. Both near-field and far-field ground motions are considered in this study. A near-field motion is considered to be a pulse-type motion. On the other hand, a far-field ground motion is considered to represent a long-duration motion with a specific, mostly broad-banded, frequency content and bandwidth, where the strong-motion phase is initiated after a few cycles of motion. The effect of far-field ground motion parameters, such as the frequency content and bandwidth, intensity, time to initiation, and duration of ground motion, on the ability of a TLD to control the earthquake response of a structure is studied. This essentially provides an insight into the manner in which a TLD controls the structural response.

PROBLEM FORMULATION

1. Structure Idealization

A single-degree-of-freedom (SDOF) structure with a TLD attached to it and subjected to a ground motion is shown in Figure 1. The equation of motion for this SDOF structure is

$$m_s\ddot{u}_x + c_s\dot{u}_x + k_s u_x = -m_s\ddot{u}_g + F \quad (1)$$

where m_s, k_s and c_s represent the mass, stiffness and damping of the structure, respectively. Moreover, u_x is the displacement of the structure relative to the ground, $\ddot{u}_g$ is the ground acceleration, and F denotes the shear force developed at the base of the TLD due to water sloshing. Equation (1), when normalized with respect to the structural mass, is expressed as

$$\ddot{u}_x + 2\xi_s\omega_s\dot{u}_x + \omega_s^2 u_x = -\ddot{u}_g + \frac{F}{m_s} \quad (2)$$

where ω_s (= $2\pi/T_s$) and ξ_s are the natural frequency and damping ratio respectively of the structure, and T_s is the natural period. The base shear force F, acting on the TLD and shown on the right hand side of Equation (2), is determined by solving the equations of motion of water in the TLD. The primary structure considered is a shear-beam structure with stiffness k_s, mass m_s and damping ratio ξ_s, as shown in Figure 1. There is no secondary structure as such and the TLD is rigidly connected at the top of the (shear-beam) structure. The design of the TLD is done as per the procedure discussed by Banerji et al. (2000). The mass of the TLD is taken as 1%, 2% and 4% of the mass of the structure, and accordingly the number of TLDs is calculated. The mass of the structure is taken as 10,000 kg and two different damping ratios are considered as ξ_s = 2% and 5%.

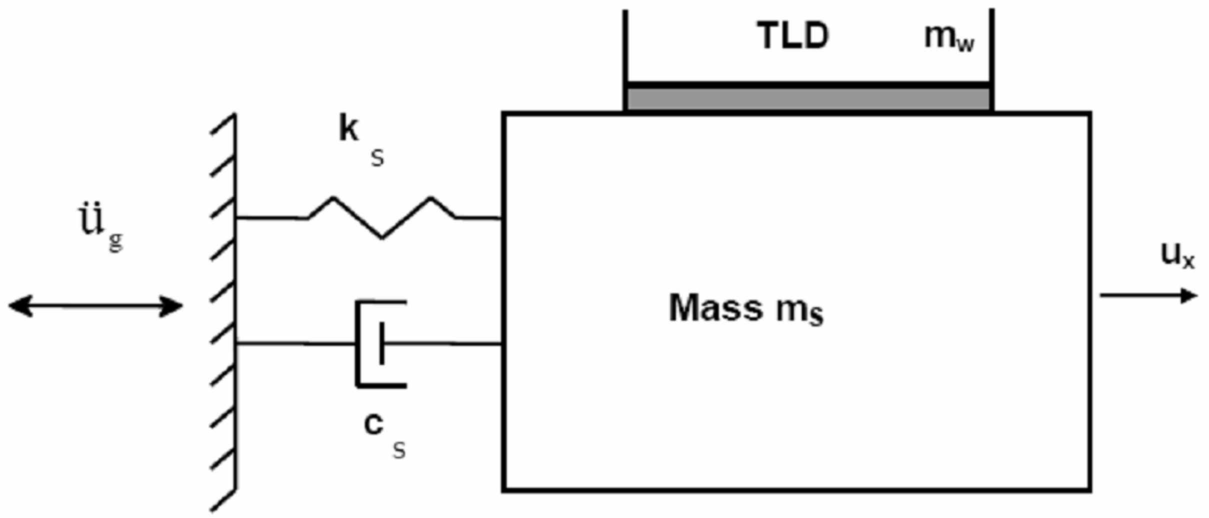

Fig. 1 Shear-beam structure with TLD

2. Formulation of TLD Equations

As shown in Figure 2. the rigid, rectangular TLD tank has a length $2a$, width b (not shown in the figure), and an undisturbed water depth h. It is subjected to the lateral base displacement x_s, which is identical to the displacement at the top of the structure. The equations of motion of water inside the tank can be defined in terms of the free-surface motion, as the water is assumed to be shallow in depth (Sun et al., 1989). Since a strong earthquake ground motion generally results in a large-amplitude excitation to the TLD, the equations of motion should include the effects of wave breaking. Considering the formulation of Sun et al. (1992), the governing equations of motion of the water become

$$\frac{\partial \eta}{\partial t} + h\sigma \frac{\partial(\phi u)}{\partial x} = 0 \tag{3}$$

$$\frac{\partial u}{\partial t} + \left(1 - T_H^2\right) u \frac{\partial u}{\partial x} + C_{fr}^2 g \frac{\partial \eta}{\partial x} + gh\sigma\phi \frac{\partial^2 \eta}{\partial x^2} \frac{\partial \eta}{\partial x} = -C_{da}\lambda u - \ddot{x}_s \tag{4}$$

where $\eta(x,t)$ and $u(x,\eta,t)$ are dependent variables. Those denote the free-surface elevation above the undisturbed water level and the horizontal free-surface water particle velocity, respectively. However, in the solution of TLD equations, $u(x,t)$ is considered, because the variation of u with the height of wave is neglected. Both of these variables are a function of the horizontal distance x from o (see Figure 2) and time t. The horizontal acceleration of the base of TLD, which is identical to the total acceleration of the top of the structure, is $\ddot{x}_s$ (as the TLD is rigidly connected to the top of structure), and the acceleration due to gravity is g. Equation (3) represents the integrated form of the continuity equation for water, and Equation (4) is derived from the two-dimensional Navier-Stokes equation. The parameters, σ, ϕ and T_H, in Equations (3) and (4) are given by the expressions (Chaiseri et al., 1989),

$$\begin{aligned} \sigma &= \tanh kh / kh \\ \phi &= \tanh k(h+\eta) / \tanh kh \\ T_H &= \tanh k(h+\eta) \end{aligned} \tag{5}$$

where k is the wave number. In Equation (4) λ is a damping parameter that accounts for the effects of the boundary layer along the tank bottom and side walls and the free-surface contamination of the water. This can be expressed semi-analytically as (Chaiseri et al., 1989)

$$\lambda = \frac{1}{(\eta + h)} \frac{1}{\sqrt{2}} \sqrt{\omega_l \nu} \left[1 + \frac{2h}{b} + s\right] \tag{6}$$

in which ω_l is the fundamental linear sloshing frequency of water in the tank, ν denotes the kinematic viscosity of water, and s denotes a surface contamination factor which can be taken as unity (Fujino et al., 1992). The fundamental linear sloshing frequency of the TLD is given by (Chaiseri et al., 1989)

$$\omega_l = \sqrt{\frac{\pi g}{2a} \tanh \pi\Delta} \tag{7}$$

where Δ is the ratio of undisturbed water depth h to the tank length $2a$, called as the water-depth ratio in this paper.

The coefficients C_{fr} and C_{da} in Equation (4) are incorporated to modify the wave phase velocity and damping of water, respectively, when the waves are unstable (i.e., $\eta > h$) and they break (Sun et al., 1992). These coefficients assume the unit value when the waves do not break. Conversely, when the waves break, C_{fr} is found empirically (Sun et al., 1992) to essentially have a constant value of 1.05, whereas C_{da} has a value which is dependent on the amplitude $(x_s)_{\max}$ of the motion of the top of the structure when it does not have a TLD attached to it. The value of C_{da} is obtained as (Sun et al., 1992)

$$C_{da} = 0.57\sqrt{\frac{h^2\omega_l}{a\nu}(x_s)_{\max}} \tag{8}$$

where, as before, h and a are the water depth and half tank length, respectively, and ω_l is the sloshing frequency given by Equation (7).

By solving Equations (3) and (4) simultaneously for the free surface elevation η and neglecting higher-order terms and shear stresses along the bottom of the tank, a reasonable estimate of the shear force F at the base of the TLD is obtained as (Chaiseri et al., 1989; Sun et al., 1992)

$$F = \frac{\rho g b}{2}\left[(\eta_n + h)^2 - (\eta_0 + h)^2\right] \tag{9}$$

where ρ is the mass density of water, b is the tank width, and η_n and η_0 are the free-surface elevations at the right and left walls, respectively, of the tank.

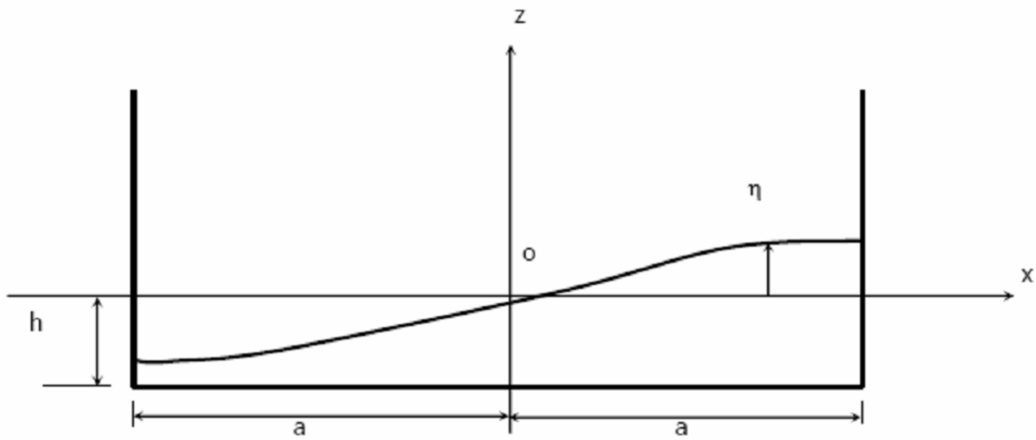

Fig. 2 Schematic sketch of TLD for horizontal motion

3. Solution of Equations of Motion

Equations (2)–(4) have to be solved simultaneously to find the response of a SDOF structure with a TLD attached. Although the behavior of the structure is linear, the motion of water is nonlinear. Therefore, an iterative numerical procedure is needed to compute the response of the structure. Equations (3) and (4) are discretized, with respect to x, into difference equations and then those are solved by using the standard Runge-Kutta-Gill procedure. Equation (2) is solved by using a central difference scheme, in which the time step depends on defining the sloshing phenomenon properly but is also small enough to ensure numerical stability.

DEFINITION OF GROUND MOTIONS

For carrying out a comprehensive study of the effect of a TLD on structural response when subjected to a ground motion, it is necessary to consider all the possible types of earthquake motions. A ground motion is typically characterized by its intensity, frequency content and strong-motion duration. To this end, two different types of ground motions are considered in this study: pulse motions and long-duration random motions. The first type of motion considered is a pulse motion of extremely short duration. This type of motion mostly characterizes the earthquake motions recorded near a causative fault, i.e., in near field. The second type of motion considered is the standard random motion of intermediate-to-long duration, which characterizes earthquake motions recorded far from the causative fault, i.e., in far field.

1. Pulse-Type Motions

In order to assess the effectiveness of TLDs in controlling the seismic response of structures that are situated close to an epicentre, the pulse type of motions are considered in the present study. As stated earlier, this type of motions represents actual near-field motions. In this study, both recorded and artificially simulated pulse-type motions are considered. A near-field ground motion recorded at the Sylmar station during the 1994 Northridge earthquake is considered in the present study. The velocity time histories of the fault-parallel and fault-normal motions are presented in Figure 3. It is clear that the fault-normal component is a pulse-type motion. To understand the nature of TLD-structure interaction for the pulse-type motions, artificially generated pulse motions as described by Makris (1997) are also considered in this study. Three different types of pulse motions are taken, denoted as Type-A, Type-B and Type–C2 motions and approximated by simple trigonometric functions.

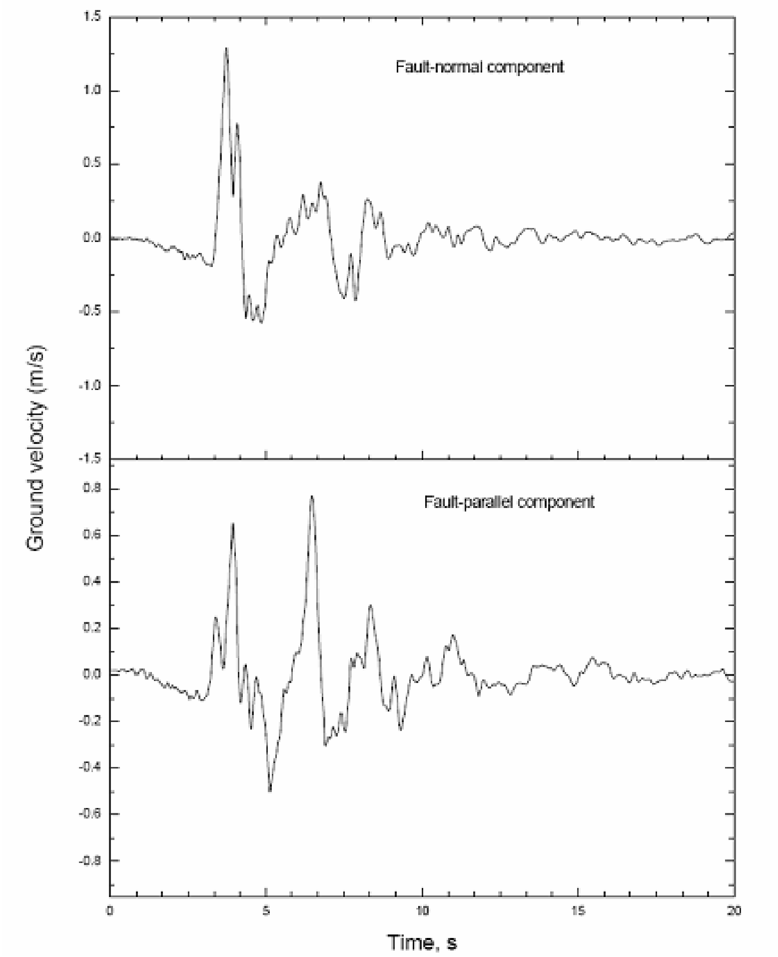

Fig. 3 Velocity time histories of the fault-normal and fault-parallel components of Sylmar record of 1994 Northridge earthquake

The analytical expression of ground acceleration of a Type-A pulse motion is given by

$$\ddot{u}_g\left(t\right)=\omega_p\frac{v_p}{2}\sin\omega_p t;\quad 0\le t\le T_p \tag{10}$$

where v_p is the amplitude of velocity pulse, and T_p ($=2\pi/\omega_p$) is the predominant period and duration of the pulse. In the present study, $v_p = 1$ m/s and $T_p = 1$ s are considered.

For the Type-B pulse motion, the analytical expression for ground acceleration is given by

$$\ddot{u}_g\left(t\right)=\omega_p v_p\sin\left(\omega_p t+\frac{\pi}{2}\right);\quad 0\le t\le T_p \tag{11}$$

where the values of v_p and T_p are considered as 1 m/s and 1 s, respectively, for the present study.

The near-fault ground motions, where the displacement history exhibits one or more long-duration cycles, are approximated by a Type-C pulse. An n-cycle ground acceleration time history is approximated by a Type-Cn pulse defined as

$$\ddot{u}_g(t) = \omega_p v_p \sin\left(\omega_p t + \varphi\right); \quad 0 \le t \le \left(n + \frac{1}{2} - \frac{\varphi}{\pi}\right) T_p \tag{12}$$

where v_p and T_p are same as defined earlier, and φ is the phase angle, the value of which is determined by the requirement that ground displacement at the end of the pulse be zero. For a Type-C2 pulse, the value of φ is found to be $0.041\pi^7$. In the present study, the values of v_p and T_p are taken as 1 m/s and 1 s, respectively. The acceleration time histories for all of these pulse-type motions are shown in Figure 4.

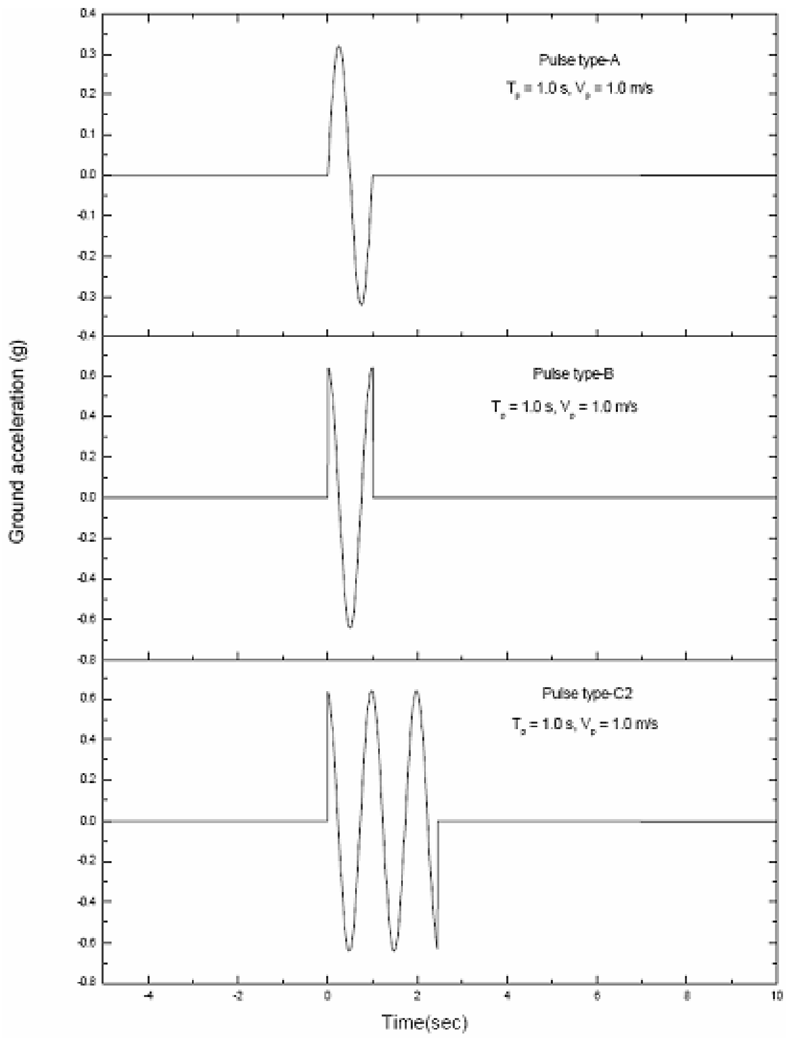

Fig. 4 Ground acceleration time histories for three idealized pulse-type ground motions

2. Long-Duration Random Earthquake Motions

The long-duration random earthquake motions are considered to study the behaviour of a structure with a TLD attached when subjected to the far-field earthquake ground motions, and to investigate the effectiveness of a TLD in controlling the seismic response of a structure. There is, however, a difficulty with studying the effectiveness of a TLD for individual ground motions, which typically have uneven response spectra (Banerji et al., 2000). This can be overcome by evening out the response spectra over a frequency spectrum. One approach is to take many recorded accelerograms, each normalized to an identical value of peak ground acceleration, and to consider the mean structural response. Another approach is to take a significant number of spectrum-compatible, artificially generated accelerograms and to consider the mean structural response. The advantage of the second approach is that the frequency content and bandwidth of the earthquake ground motion can be varied to represent an ensemble of ground motions for different types of soil conditions (Ruiz and Penzien, 1969; Der Kiureghian, 1996).

In the present study, both the approaches have been followed to assess the effectiveness of TLDs for controlling the seismic response of a structure. In the first approach, 30 different recorded accelerograms are selected and each one of those is normalized to a peak ground acceleration of 0.35*g*, which is approximately the same intensity as that of the El Centro ground motion. The list of these ground motions along with their individual peak ground accelerations is given in Table 1. In the second approach, different sets of 20 accelerograms are generated and the mean response of the structure for each set is obtained. A numerical procedure is used to generate the digital records of artificial earthquakes (Ruiz and Penzien, 1969) from the time-modulated Kanai-Tajimi spectrum by defining particular values for its frequency parameter ω_g and damping parameter ξ_g. Eight sets of artificial accelerograms are generated in order to study the effect of ground motion parameters on the ability of a TLD to control the earthquake response of a structure. The filter parameters and shaping function time parameters for these sets of ground motions are given in Table 2. It may be noted that the datum ground motion is a Set-I motion, corresponding to $\omega_g = 2\pi$ rad/s, $\xi_g = 0.4$, $t_i = 2$ s, $t_{sd} = 11$ s and $t_d = 30$ s, and that all the other sets are the variations of this set as described in Table 2.

Table 1: List of Far-Field Recorded Earthquake Ground Motions

Earthquake	Station Name	Component	PGA (*g*)
1989 Loma Prieta	Foster City Redwood Shores	0^o	0.258
	Gilroy # 2—HWY 101/Bolsa Rd Motel	0^o	0.351
	Hayward—Bart Station	220^o	0.156
	Hollister—Sago South Cienega Rd	261^o	0.072
	Hollister—South Street and Pine Drive	0^o	0.369
	Richmond—City Hall Parking Lot	190^o	0.125
	San Francisco Bay—Dumbarton Bridge	267^o	0.129
	Woodside—Fire Station	0^o	0.099
	Capitola—Fire Station	0^o	0.472
	San Franscisco International Airport	0^o	0.235
	Yerba Buena Island	0^o	0.029
	Coyote Lake Dam—Downstream	195^o	0.158
	Gilroy # 6—San Ysidro	90^o	0.170
	Olema—Point Reyes Ranger Station	90^o	0.102
	Agnew—Agnews State Hospital	0^o	0.166
	San Francisco—Diamond Heights	0^o	0.098
1994 Northridge	New Hall LA Country Fire Station	360^o	0.308
	Camarillo	180^o	0.125
	Alhambra—Fremont School	360^o	0.080
	Los Angeles—Baldwin Hills	90^o	0.239
	Los Angeles—Hollywood Storage Grounds	90^o	0.231
	Los Angeles—Obergon Park	90^o	0.355
	Mt Wilson—Caltech Seismic Station	90^o	0.133
	Pacoima—Kagel Canyon	90^o	0.300
	Point Mugu—Naval Air Station	90^o	0.143
	Rolling Hills Estates—Rancho Vista Sch	90^o	0.116
	Sanpedro—Palos Verdes	90^o	0.095
	Vasquez Rocks Park	360^o	0.151
	Lake Hughes # 9	90^o	0.225
1987 Whitter	Inglewood—Union Oil Yard	220^o	0.156

A comparison of the mean pseudo-acceleration spectra for the recorded ground motions (on hard soil) and artificially generated ground motions for hard soil is presented in Figure 5. The relatively close match between the two mean spectra illustrates the validity of the subsequent study based on only the artificial accelerograms.

Table 2: Filter Parameters and Shaping Function Time Parameters for Various Sets of Artificially Generated Ground Motions

Set No.	ω_g (rad/s)	ξ_g	t_i (s)	t_{sd} (s)	t_d (s)	PGA (g)
I	2.0π	0.4	2	11	30	0.35
II	1.5π	0.4	2	11	30	0.35
III	3.0π	0.4	2	11	30	0.35
IV	2.0π	0.2	2	11	30	0.35
V	2.0π	0.6	2	11	30	0.35
VI	2.0π	0.4	2	4	30	0.35
VII	2.0π	0.4	2	11	30	0.5
VIII	2.0π	0.4	2	11	30	1.0

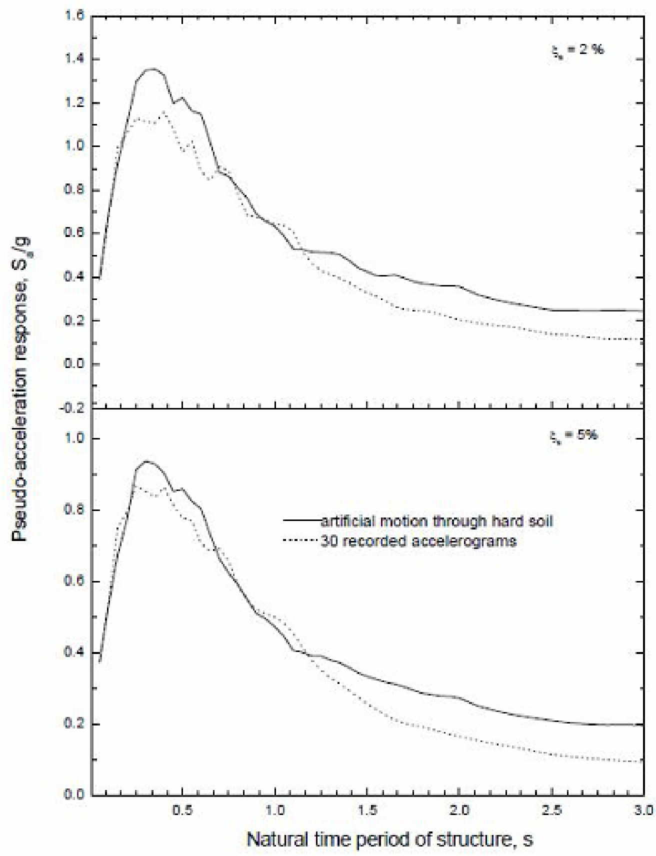

Fig. 5 Comparison of mean pseudo-acceleration response spectra for artificially generated ground motions for hard soil and 30 recorded accelerograms

RESPONSE OF STRUCTURES TO GROUND MOTIONS

1. Response to Pulse-Type Motions

Figure 6 compares the time histories of the total acceleration response of a typical structure with and without TLD for both the components of the Sylmar ground motion of the 1994 Northridge earthquake. The fault-normal component is a short-duration pulse-type motion with the peak ground acceleration occuring in the first pulse (see Figure 3), and it may be observed that the TLD is not effective as it does not get a chance to dissipate energy. The fault-parallel component is relatively a longer-duration ground motion with the peak ground acceleration occuring after a few seconds of strong motion and therefore the TLD is clearly more effective in this case.

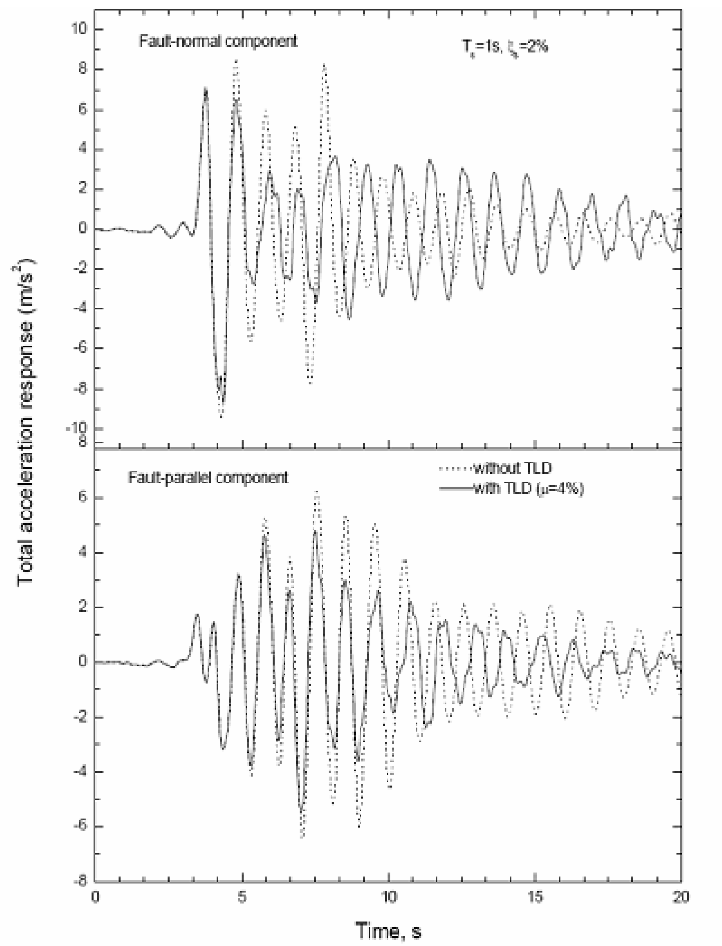

Fig. 6 Total acceleration response time histories of a typical structure, with and without TLD, when subjected to the two components of Sylmar motion of 1994 Northridge earthquake

A more detailed study of TLD-structure interaction for the pulse-type motions is done by considering the three idealized pulse motions shown in Figure 4. Peak responses at the top of a typical structure due to the Type-A, Type-B and Type-C2 motions and percentage reductions in those due to the TLD of varying mass ratios are presented in Table 3. From this table, it is seen that the TLD is not significantly effective for the Type-A pulse motion, as compared to the Type-B and Type-C2 pulse motions. The reason behind this can be traced from the comparisons of the typical time-history plots for total acceleration at the top of a representative structure with and without TLD as shown in Figure 7 for the three pulse motions. It is seen that since the Type-A pulse is of extremely short duration, the peak response occurs in the very first cycle itself. Therefore, for this pulse motion, the TLD, in which the sloshing has just started, does not get a chance to dissipate energy and thus proves to be ineffective. For the Type-B pulse, the peak occurs in the second cycle and is of higher intensity than that for the Type-A pulse, and therefore the TLD is obviously more effective. The Type-C2 pulse is of relatively longer duration and the peak occurs after a few cycles. Therefore, in this case, the TLD gets more time to dissipate energy and is consequently most effective. Thus, it can be concluded that a TLD is effective for the pulse-type motions only if the peak response of the structure occurs more than two cycles of vibration after the start of the strong motion.

Table 3: Peak Responses at the Top of a Typical Structure, Due to Pulse Ground Motions, and Percentage Reductions in Those Due to a TLD of Varying Mass Ratios

Type of Ground Motion	$(a_{max})_0$ (m/s^2)	Percentage Reduction in a_{max}		
		$\mu = 1\%$	$\mu = 2\%$	$\mu = 4\%$
Type-A	9.29	3.34	5.59	8.83
Type-B	18.37	4.08	7.89	15.19
Type-C	39.76	10.49	16.0	24.0

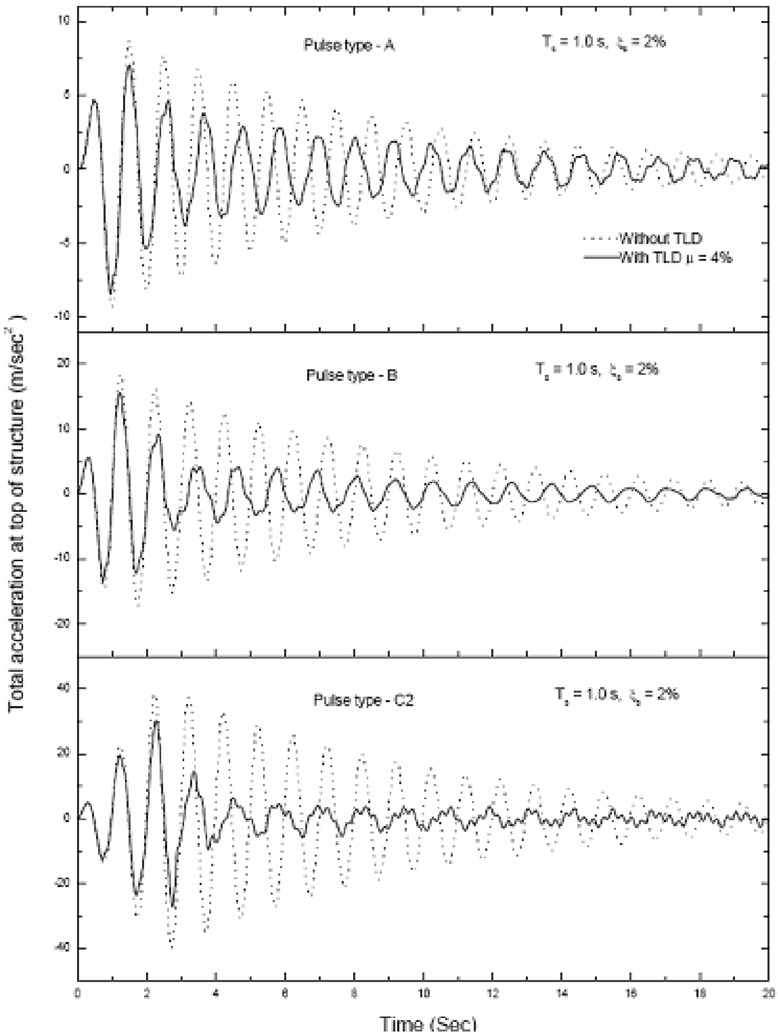

Fig. 7 Total acceleration response time histories of a typical structure, with and without TLD, when subjected to the three idealized pulse ground motions

2. Response to Long-Duration Ground Motions

The mean peak total acceleration responses at the top of certain representative structures, due to the 30 recorded accelerograms listed in Table 1 and scaled to the peak ground acceleration of 0.35*g*, and percentage reductions in those due to a TLD of mass ratio of 4% are presented in Table 4. The same results for the artificially generated ground motions for hard soil are also presented in this table. From this comparison, it is seen that the TLD is effective across the spectrum of structural frequencies considered for both actual and artificial ground motions and that the level of effectiveness is approximately the same for both types of ground motions. For the recorded motions, it is seen that on average the TLD reduces 25% of the response for 2% structural damping, while it reduces 15% response for 5% structural damping. For a specific structure of 0.75-s period, the response reduction is as much as 32% for 2% structural damping and about 20% for 5% structural damping. This shows that a TLD is indeed effective in controlling the earthquake response of structures. Furthermore, this illustrates the fact that a TLD becomes progressively less effective as the structural damping increases, since the overall effect of the added viscous damping due to sloshing in the TLD gets reduced.

A TLD absorbs and dissipates energy based on the level of sloshing and wave breaking and, irrespective of the amount of structural damping; this energy dissipation remains the same for a particular excitation level of the TLD. The base motion of the TLD is $\ddot{x}_s$ which is same as the total acceleration of the top of the structure. As the base motion decreases, sloshing action in the TLD is reduced and hence its effectiveness reduces. As the structural damping is increased, total acceleration at the top of the structure is reduced and hence the base motion of the TLD also reduces. This results in less sloshing and therefore the effectiveness of TLD reduces. For a particular amount of sloshing, the added damping is constant. For 2% structural damping, the damping added by the TLD is thus higher than that for 5% structural damping, though the structure is subjected to same excitation in both cases. For a structure having larger structural damping, the damping added by energy dissipation in the TLD is smaller as a fraction of the overall damping. Thus, the effectiveness of TLD is reduced. The effectiveness of TLD increases with mass ratio due to the increased sloshing action. For 5% damping, a TLD with the mass ratio of 2% will not be effective. Therefore in this study, for 2% damping, the mass ratio of TLD is considered as 2%, while for 5% damping, the mass ratio is considered as 4%.

Table 4: Mean Peak Responses at the Top of Representative Structures, Due to 30 Recorded Far-Field Motions and Artificial Motions for Hard Soil, and Percentage Reductions in Those Due to a TLD with 4% Mass Ratio

Structural Properties		Response Due to 30 Recorded Far-Field Motions		Response Due to Artificial Motions for Hard Soil	
T_s (s)	ξ_s (%)	$(a_{\max})_0$ (m/s^2)	Percentage Reduction in $a_{\max}$	$(a_{\max})_0$ (m/s^2)	Percentage Reduction in $a_{\max}$
0.5	2.0	9.68	21.8	12.21	36.5
	5.0	7.75	15.35	8.57	22.5
0.67	2.0	8.47	17.71	9.33	28.0
	5.0	6.83	12.74	6.98	21.6
0.75	2.0	8.77	32.38	8.53	29.8
	5.0	6.53	19.90	6.19	18.9
1.0	2.0	6.34	22.08	6.26	28.0
	5.0	4.94	14.98	4.68	18.8
1.5	2.0	3.24	20.68	4.19	22.7
	5.0	2.55	12.16	3.30	14.6
2.0	2.0	2.03	20.20	3.52	26.1
	5.0	1.64	13.41	2.70	17.8

EFFECT OF GROUND MOTION PARAMETERS

Ground motions are characterized by various parameters. The following are those important parameters which affect the behaviour of structures when they are subjected to earthquake ground motions:

a) frequency content and bandwidth of ground motion,
b) duration of stationary intensity of ground motion, and
c) intensity of ground motion.

1. Effect of Frequency Content and Bandwidth

In order to study the effect of frequency content of ground motion, three sets of ground motions are generated with different central frequencies, keeping other parameters constant. The central frequencies considered are $\omega_g = 1.5\pi$, 2π and 3π rad/s (i.e., corresponding to the Set-II, Set-I and Set-III motions in Table 3).

To study the effect of frequency bandwidth of ground motion, three sets of ground motions with different bandwidth parameters are again generated, while keeping the other parameters constant. The bandwidth parameters considered are ξ_g = 0.2 (narrow), 0.4 (medium) and 0.6 (broad) (i.e., corresponding to the Set-IV, Set-I and Set-V motions in Table 2).

The percentage reductions by a TLD in the mean peak acceleration responses at the top of various structures for the above sets of ground motions are shown in Table 5. From this table, it can be seen that the TLD is more effective for those structures whose natural frequencies are close to the central frequency of ground motion and thus the structural response is very large anyway. Around the central frequency of ground motion, the effectiveness of TLD increases as the central frequency of ground motion increases. For ω_g = 1.5π rad/s (or T_g = 1.33 s) and T_s = 1.33 s, the reduction in response is 22%; for ω_g = 2.0π rad/s (or T_g = 1.0 s) and T_s = 1.0 s, the reduction in response is 24.94%; and for ω_g = 3.0π rad/s (or T_g = 0.67 s) and T_s = 0.67 s, the reduction in response is 27.94% (with the structural damping remaining unchanged at 2%). The reasoning for this kind of behavior of TLD is that as the central frequency of ground motion increases, the base acceleration of TLD is higher, thus leading to a greater sloshing action as stated above. A TLD can thus become more effective even when the tuning is not perfect.

Table 5: Percentage Reductions in Mean Peak Acceleration Responses at Top of Various Structures Due to a TLD (with $\mu = 2\%$ for $\xi_s = 2\%$ and $\mu = 4\%$ for $\xi_s = 5\%$) for Different Sets of Ground Motions with Varying Central Frequencies and Varying Bandwidths

Structural Properties		Percentage Reductions in Mean Peak Accelerations for					
		Ground Motions with Different Central Frequencies			Ground Motions with Different Bandwidth Parameters		
T_s (s)	ξ_s (%)	$\omega_g = 1.5\pi$ ($T_g = 1.33$ s)	$\omega_g = 2.0\pi$ ($T_g = 1.0$ s)	$\omega_g = 3.0\pi$ ($T_g = 0.67$ s)	$\xi_g = 0.2$	$\xi_g = 0.4$	$\xi_g = 0.6$
0.5	2.0	13.71	16.44	28.54	9.45	16.44	20.99
	5.0	8.58	8.59	13.01	1.37	8.59	8.67
0.67	2.0	9.30	15.98	27.94	8.79	15.98	18.5
	5.0	3.69	7.82	17.22	1.17	7.82	10.93
0.75	2.0	11.99	16.23	24.03	10.67	16.23	17.78
	5.0	4.15	8.58	19.27	−0.85	8.58	11.94
1.0	2.0	19.64	24.94	23.33	29.95	24.94	23.44
	5.0	8.54	18.94	22.21	21.49	18.94	19.59
1.33	2.0	22.0	22.29	18.66	24.13	22.29	20.23
	5.0	13.86	16.19	14.26	17.67	16.19	15.25
1.5	2.0	21.86	20.74	17.60	20.99	20.74	19.89
	5.0	20.20	20.63	16.55	19.52	20.63	18.93
2.0	2.0	14.03	12.03	11.97	12.12	12.03	12.31
	5.0	15.58	12.37	13.02	11.10	12.37	12.83

It may be noted here that the TLD is significantly effective even for a higher damping ratio of 5%, when the structure frequency is close to the central frequency of ground motion. Thus, it can be concluded that a TLD is more effective, when the structure frequency is close to the central frequency of ground motion and the response of the structure without TLD is large. Furthermore, a TLD is most effective for the high-frequency ground motions. This is so because TLDs basically work on two principles: (i) tuning, and (ii) sloshing. At a higher frequency, when the structure frequency is close to (but not exactly equal to) the frequency of ground motion, a TLD is subjected to more sloshing, and hence more energy dissipation takes place. Unlike a TLD, a TMD is effective only when the frequency ratio is unity. It can be seen from Table 5 that at ω_g = 3.0π rad/s (or T_g = 0.67 s), the effectiveness of a TLD is maximum for the structures having periods from 0.5 to 1.0 s, as compared to the effectiveness of a TLD for the same structures but with ω_g = 2.0π and 1.5π rad/s (i.e., with T_g = 1.0 and 1.33 s).

As stated earlier, the effectiveness of a TLD is primarily due to the sloshing action rather than tuning. The sloshing action is more whenever the base motion of the TLD is higher and is more effective even though tuning is not perfect. For instance in Table 5, for the 0.5-s structure, the base motion is higher than that for the 0.67-s structure. Hence, the TLD is more effective for the 0.5-s structure compared to the 0.67-s structure, even though the TLD is tuned to the 0.67-s structure as in Banerji et al. (2000).

The parameter ξ_g represents the bandwidth of ground motion. Table 5 shows the reductions in structure response for the ground motions with different bandwidth parameters, ξ_g = 0.2, 0.4 and 0.6, but for a constant central frequency, $\omega_g = 2.0\pi$ rad/s (i.e., for the Set-IV, Set-V and Set-VI motions). It is clear from these results that a TLD is more effective for the 1-s structure for all bandwidths and that this effectiveness is maximum for ξ_g = 0.2. As mentioned earlier, the effectiveness of a TLD broadly depends on the sloshing action. At these parameters, the TLD is subjected to the maximum base motion and hence is found to be more effective.

It may also be seen from Table 5 that for the broad-banded motions, the TLD is effective over a broad spectrum of structural frequencies, whereas for the narrow-banded ground motions, the TLD is effective only if the structural frequency is in the vicinity of the central frequency of ground motion. However, it should be noted that for the structures with natural frequencies in the vicinity of the central frequency of ground motion, the effectiveness of TLD increases as the bandwidth of ground motion decreases. For example, the response reduction is fairly constant at around 20% across the spectrum of structural frequencies for the broad-banded ground motions, whereas for the narrow-banded ground motions, the response reduction varies from around 30% for the 1-s structure to around 9% for the 0.5-s structure. The reason for the above behaviour can be traced to the fact that the narrow-banded ground motions tend to become harmonic ground motions, for which a TLD is effective only if the frequencies of the structure, TLD and excitation are very close to each other.

According to Der Kiureghian (1996), as the soil becomes softer, the central frequency ω_g and bandwidth ξ_g are reduced. Hence, for softer soils, a TLD will be increasingly more effective for a structure whose natural frequency is close to the central frequency of ground motion, but will be significantly less effective for those structures whose frequencies are away from the central frequency of ground motion. It has already been stated in this paper that the effectiveness of a TLD reduces with an increase in the structural damping but is not significantly affected by the structure frequency for the broad-banded ground motions. It is, of course, assumed here that the TLD for each structure is designed as per the procedure given in Banerji et al. (2000). Thus, the TLD properties, except for the mass ratio, vary with the natural frequency of structure.

2. Effect of Duration of Stationary Intensity

In this study two different sets of ground motions with different values of t_{sd} are considered. One set is having t_{sd} = 11 s (corresponding to the Set-I motion in Table 2), while the other set is having t_{sd} = 4 s (corresponding to the Set-VI motion in Table 2). The percentage reductions in the mean peak responses at the top of various structures due to a TLD for these sets of ground motions are shown in Table 6. From these results, it can be seen that for the relatively short-period structures, the duration of the stationary intensity of ground motion does not have significant effect on the performance of TLD. However, for the relatively long-period structures, the TLD is more effective for the ground motions having a longer duration of strong motion. This is because in the case of the ground motions with a short duration of strong motion, the short-period structures get a chance to vibrate for at least a few cycles within the strong-motion duration, while for the long-period structures, the 4-s strong-motion duration motion becomes like a pulse-type motion.

3. Effect of Ground-Motion Intensity

In order to study the effect of the intensity of ground motion, three different sets of ground motions with varying intensities are generated, while keeping the other parameters unchanged. The peak ground accelerations (PGAs) considered for these motions are 0.35*g*, 0.5*g* and 1.0*g* (corresponding to the Set-I, Set-VII and Set-VIII motions in Table 2). The mean peak total acceleration responses at the top of various structures due to these sets of ground motions and percentage reductions in those due to a TLD are presented in Table 7. From this table, it is clear that the TLD is more effective as the intensity of ground excitation increases. This is a highly desirable property of the TLD, which essentially behaves as a nonlinear viscous damper. The reason for this can be traced to the basic energy dissipation mode for a TLD. At a higher ground-excitation intensity, the TLD is subjected to a larger base motion; this results in a greater amount of sloshing with wave breaking taking place, which increases energy dissipation in the

TLD. However, it is to be noted here that at a further higher level of excitation (say, of 1.0*g* peak ground acceleration), the sloshing-slamming phenomenon takes place. An experimental study on TLDs at high levels of excitation by Banerji et al. (2010) has shown that this phenomenon results in greater energy dissipation. Hence, at the higher levels of excitation, a TLD becomes in reality much more effective than that predicted by the present numerical model.

Table 6: Percentage Reductions in Mean Peak Acceleration Responses at Top of Various Structures Due to a TLD (with $\mu = 2\%$ for $\xi_s = 2\%$ and $\mu = 4\%$ for $\xi_s = 5\%$) for Artificial Ground Motions with Varying Durations of Stationary Intensity t_{sd}

Structural Properties		Percentage Reduction in Mean Peak Acceleration	
T_s (s)	ξ_s (%)	$t_{sd} = 11$ s	$t_{sd} = 4$ s
0.5	2.0	16.44	16.23
	5.0	8.59	11.01
0.67	2.0	15.98	15.24
	5.0	7.82	7.95
0.75	2.0	16.23	13.89
	5.0	8.58	11.02
1.0	2.0	24.94	20.84
	5.0	18.94	20.89
1.33	2.0	22.29	11.94
	5.0	16.19	13.01
1.5	2.0	20.74	15.64
	5.0	20.63	15.30
2.0	2.0	12.03	8.39
	5.0	12.37	10.38

Table 7: Mean Peak Total Acceleration Responses at Top of Various Structures, Due to Different Sets of Ground Motions of Varying Intensities (i.e., PGAs), and Percentage Reductions in Those Due to a TLD (with $\mu = 2\%$ for $\xi_s = 2\%$ and $\mu = 4\%$ for $\xi_s = 5\%$)

Structural Properties		Mean Peak Total Acceleration at Top of Structures without TLD, $(a_{\max})_0$ (m/s^2)			Percentage Reduction in Mean Peak Total Acceleration Due to TLD		
T_s (s)	ξ_s (%)	0.35*g*	0.5*g*	1.0*g*	0.35*g*	0.5*g*	1.0*g*
0.5	2.0	9.77	13.96	27.92	16.44	16.36	20.63
	5.0	7.75	11.07	22.14	8.59	8.05	8.28
0.67	2.0	12.54	17.91	35.82	15.98	20.50	28.33
	5.0	9.43	13.48	26.95	7.82	9.07	16.30
0.75	2.0	12.34	17.62	35.24	16.23	19.68	28.23
	5.0	9.59	13.70	27.39	8.58	9.01	17.90
1.0	2.0	13.84	19.78	39.55	24.94	28.40	34.89
	5.0	10.30	14.71	29.43	18.94	18.97	25.52
1.33	2.0	10.38	14.83	29.65	22.29	25.32	31.25
	5.0	7.75	11.07	22.14	16.19	17.16	24.56
1.5	2.0	9.36	13.37	26.74	20.74	22.86	29.02
	5.0	7.14	10.20	20.41	20.63	21.11	26.75
2.0	2.0	6.43	9.19	18.37	12.03	14.16	18.29
	5.0	5.23	7.47	14.94	12.37	14.38	16.79

SUMMARY AND CONCLUSIONS

A comprehensive study on the effectiveness of a TLD in controlling the earthquake response of structures has been carried out by considering various types of ground motions. It has been found that though the TLD adds damping to the structure, it is not effective in reducing the response of structures for the extremely short-duration pulse-type motions. However, if the pulse duration is long enough for the peak response to occur after at least two cycles of structural vibration, the TLD becomes progressively more effective. For the longer-duration ground motions, the TLD has been found to be quite effective. It has also been shown that the artificially generated ground motions considered in this study accurately reflect the characteristics of recorded ground motions. Finally, by varying the parameters of the artificially generated ground motions, the effect of ground motion parameters on the effectiveness of a TLD in reducing the structural response has been investigated. An interesting point that needs recapitulation here is that a TLD becomes increasingly more effective as the ground-motion intensity increases. Therefore, a TLD is one passive vibration control device that is more effective for the more intense ground motions.

NOTATIONS

a	=	half the tank length of TLD
$(a_{\max})_0$	=	mean peak total acceleration at the top of shear-beam structure
b	=	width of TLD tank
c_s	=	damping coefficient of shear-beam structure
C_{da} and C_{fr}	=	coefficients to account for wave breaking in TLD
c	=	wave speed/constant used in ground motion intensity function
F	=	resultant base shear in TLD in global X-direction
g	=	acceleration due to gravity
h	=	water depth in TLD tank
k_s	=	stiffness of shear-beam structure
m_s	=	mass of shear-beam structure
s	=	surface contamination factor
T_p	=	predominant period
t	=	time (in s)
t_i	=	duration of the parabolic build-up of ground motion
t_{sd}	=	duration of the stationary intensity of ground motion
t_d	=	total duration of ground motion
$(u_{\max})_0$	=	mean peak displacement at the top of shear-beam structure
$\ddot{u}_g$	=	ground acceleration
u_s	=	velocity component at the free surface in X-direction
u_x	=	translation at the top of structure (for shear-beam/cantilever structure)
$\dot{u}_x$	=	velocity at the top of structure (for shear-beam/cantilever structure)
$\ddot{u}_x$	=	total acceleration at the top of structure (for shear-beam/cantilever structure)
v_p	=	amplitude of the velocity of pulse-type motions
x	=	horizontal distance from the centre of TLD

x_s	=	base displacement of TLD
$(x_s)_{\max}$	=	amplitude of the motion of structure's top without TLD
$\ddot{x}_s$	=	base acceleration of TLD
Δ	=	depth ratio of TLD tank
λ	=	damping parameter due to liquid sloshing
η	=	free-surface elevation of water in TLD tank
ω_g	=	frequency parameter for artificially generated ground motions
ω_s	=	natural frequency of structure
ω_l	=	fundamental sloshing frequency of TLD
ω_p	=	predominant frequency of pulse-type motions
μ	=	mass ratio
ν	=	kinematic viscosity of liquid in TLD
ξ_g	=	bandwidth parameter for artificially generated ground motions
ξ_s	=	damping ratio for shear-beam structure
ρ	=	mass density of liquid in TLD tank
φ	=	phase angle

REFERENCES

1. Banerji, P., Murudi, M., Shah, A.H. and Popplewell, N. (2000). "Tuned Liquid Dampers for Controlling Earthquake Response of Structures", Earthquake Engineering & Structural Dynamics, Vol. 29, No. 5, pp. 587–602.
2. Banerji, P., Samanta, A. and Chavan, S.A. (2010). "Earthquake Vibration Control of Structures Using Tuned Liquid Dampers: Experimental Studies", International Journal of Advanced Structural Engineering, Vol. 2, No. 2, pp. 133–152.
3. Chaiseri, P., Fujino, Y., Pacheco, B.M. and Sun, L.M. (1989). "Interaction of Tuned Liquid Damper (TLD) and Structure—Theory, Experimental Verification and Application", Structural Engineering/Earthquake Engineering, JSCE, Vol. 6, No. 2, pp. 273s–282s.
4. Den Hartog, J.P. (1956). "Mechanical Vibrations", McGraw-Hill, New York, U.S.A.
5. Der Kiureghian, A. (1996). "A Coherency Model for Spatially Varying Ground Motions", Earthquake Engineering & Structural Dynamics, Vol. 25, No. 1, pp. 99–111.
6. Fujino, Y., Sun, L., Pacheco, B.M. and Chaiseri, P. (1992). "Tuned Liquid Damper (TLD) for Suppressing Horizontal Motion of Structures", Journal of Engineering Mechanics, ASCE, Vol. 118, No. 10, pp. 2017–2030.
7. Jangid, R.S. and Kelly, J.M. (2001). "Base Isolation for Near-Fault Motions", Earthquake Engineering & Structural Dynamics, Vol. 30, No. 5, pp. 691–707.
8. Kamrani-Moghaddam, B., Rahimian, M. and Ghorbani-Tanha, A.K. (2006). "Performance of Tuned Mass Dampers for Response Reduction of Structures under Near-Field and Far-Field Seismic Excitations", Proceedings of the 4th International Conference on Earthquake Engineering, Taipei, Taiwan, Paper No. 112 (on CD).
9. Makris, N. (1997). "Rigidity-Plasticity-Viscosity: Can Electrorheological Dampers Protect Base-Isolated Structures from Near-Source Ground Motions?", Earthquake Engineering & Structural Dynamics, Vol. 26, No. 5, pp. 571–591.
10. Matta, E. (2011). "Performance of Tuned Mass Dampers against Near-Field Earthquakes", Structural Engineering and Mechanics, Vol. 39, No. 5, pp. 621–642.

11. Modi, V.J., Welt, F. and Seto, M.L. (1995). “Control of Wind-Induced Instabilities through Application of Nutation Dampers: A Brief Overview”, Engineering Structures, Vol. 17, No. 9, pp. 626–638.
12. Pinelli, J.-P., Gutierrez, H., Hu, S. and Casier, F. (2003). “Multiple Distributed Tuned Mass Dampers: An Exploratory Study”, Proceedings of the XL2003 (Response of Structures to Extreme Loading) Conference, Toronto, Canada (on CD).
13. Ruiz, P. and Penzien, J. (1969). “Probabilistic Study of the Behavior of Structures during Earthquakes”, Report EERC 69-3, University of California, Berkeley, U.S.A.
14. Sakai, F., Takaeda, S. and Tamaki, T. (1989). “Tuned Liquid Column Damper—New Type Device for Suppression of Building Vibrations”, Proceedings of the International Conference on Highrise Buildings, Nanjing, China, Vol. 2, pp. 926–931.
15. Sun, L.M., Fujino, Y., Pacheco, B.M. and Isobe, M. (1989). “Nonlinear Waves and Dynamic Pressures in Rectangular Tuned Liquid Damper (TLD)—Simulation and Experimental Verification”, Structural Engineering/Earthquake Engineering, JSCE, Vol. 6, No. 2, pp. 251s–262s.
16. Sun, L.M., Fujino, Y., Pacheco, B.M. and Chaiseri, P. (1992). “Modelling of Tuned Liquid Damper (TLD)”, Journal of Wind Engineering & Industrial Aerodynamics, Vol. 43, No. 1-3, pp. 1883–1894.
17. Tamura, Y., Fujii, K., Ohtsuki, T., Wakahara, T. and Kohsaka, R. (1995). “Effectiveness of Tuned Liquid Dampers under Wind Excitation”, Engineering Structures, Vol. 17, No. 9, pp. 609–621.
18. Taniguchi, T., Der Kiureghian, A. and Melkumyan, M. (2008). “Effect of Tuned Mass Damper on Displacement Demand of Base-Isolated Structures”, Engineering Structures, Vol. 30, No. 12, pp. 3478–3488.
19. Villaverde, R. (1994). “Seismic Control of Structures with Damped Resonant Appendages”, Proceedings of the First World Conference on Structural Control, Los Angeles, U.S.A., Vol. 1, pp. WP4-113–WP4-122.
20. Warburton, G.B. (1982). “Optimum Absorber Parameters for Various Combinations of Response and Excitation Parameters”, Earthquake Engineering & Structural Dynamics, Vol. 10, No. 3, pp. 381–401.
21. Yalla, S.K. and Kareem, A. (2000). “Optimum Absorber Parameters for Tuned Liquid Column Dampers”, Journal of Structural Engineering, ASCE, Vol. 126, No. 8, pp. 906–915.
22. Ye, K. and Li, L. (2009). “Study on the Dynamic Response of LRB Base-Isolated Structure under Near-Fault Pulse-like Ground Motions”, Earthquake Resistant Engineering and Retrofitting, Vol. 31, No. 2, pp. 32–38 (in Chinese).
23. Yu, J.-K., Wakahara, T. and Reed, D.A. (1999). “A Non-linear Numerical Model of the Tuned Liquid Damper”, Earthquake Engineering & Structural Dynamics, Vol. 28, No. 6, pp. 671–686.

ISET Journal of Earthquake Technology, Paper No. 522, Vol. 49, No. 3-4, Sept.-Dec. 2012, pp. 73–87

VARIABLE COEFFICIENT OF FRICTION: AN EFFECTIVE VFPI PARAMETER TO CONTROL NEAR-FAULT GROUND MOTIONS

Girish Malu* and Pranesh Murnal**
*Department of Civil Engineering
Dr. J.J. Magdum College of Engineering, Jaysingpur-416101
**Department of Applied Mechanics
Government College of Engineering, Aurangabad-431005

ABSTRACT

Several sliding isolation systems have been proposed to control earthquake effects. However, most of these isolation devices have limited effectiveness under the near-fault ground motions due to the pulse-type characteristics of such excitations. Recently proposed, VFPI has unique characteristics to overcome the limitations of a traditional isolation system for the near-fault ground motions. VFPI incorporates isolation, energy dissipation and restoring force mechanisms and has additional advantages due to the response-dependent variable frequency of oscillation and bounded restoring force. The device has wide choice of parameters to choose from, as per the design requirements. In this paper, the behaviour of single-storey structures isolated by using VFPI and subjected to the near-fault ground motions is numerically examined. It is shown that it is possible to increase the effectiveness of VFPI by using a discretely-varying coefficient of friction along the sliding surface. Parametric studies are carried out to critically examine the behaviour of single-storey structures isolated with the VFPI and FPS systems.

KEYWORDS: Base Isolation, VFPI, Near-Fault Ground Motions, Passive Control

INTRODUCTION

Base isolation has emerged as an effective technique in minimizing the earthquake forces. In this technique, a flexible layer (or isolator) is placed between the super-structure and its foundation such that relative deformations are permitted at this level. Due to the flexibility of the isolator layer, the time period of the motion of the isolator is relatively long; as a result, the isolator time period controls the fundamental period of the isolated structure. For a properly designed isolation system, the isolator time period is much longer than the periods containing significant ground-motion energy. As a result, the use of isolator shifts the fundamental period of the structure away from the predominant periods of ground excitation. An extensive review of the base-isolation systems and their applicability is available in literature (Buckle and Mayes, 1990; Kelly, 1993; Naeim and Kelly, 1999).

The practical isolation devices typically include an energy dissipating mechanism also, so as to reduce the deformations at the isolator level. For example, the friction-type base isolators use a sliding surface for both isolation and energy dissipation and have been found to be very effective in reducing the structural response (Mostaghel et al., 1983). Due to the characteristics of the excitation transmitted through the sliding surface, the performance of friction isolators is relatively insensitive to the severe variations in the frequency content and amplitude of the input excitation, thus making the performance of sliding isolators very robust. The simplest sliding isolator consists of a horizontal sliding surface (in the pure friction or PF system), which may experience large sliding and residual displacements. It is therefore often difficult to incorporate such an isolator in structural design.

In order to overcome the difficulty with providing restoring force, an effective mechanism to provide restoring force by gravity has been utilized in the friction pendulum systems (FPSs) (Zayas et al., 1987). In this system, the sliding surface takes a concave spherical shape so that the sliding and re-centering mechanisms are integrated into one unit. The FPS isolator has several advantages over the PF system and has demonstrated acceptable performance for many different structures and excitation characteristics (Mokha et al., 1990; Tsopelas et al., 1996; Tsai, 1997; Wang et al., 1998). However, the main disadvantage of a FPS is that it has a constant time period of oscillation due to its spherical surface. As a result, the FPS isolators can be effectively designed for a specific level (of amplitude and frequency characteristics) of the ground excitation. Under more severe ground motions, sliding displacements greater than the design displacement can occur, which may lead to very large accelerations and thus to the failure of FPS isolator. Since in a FPS isolator, the restoring force is linearly proportional to the sliding displacement, the large amount of sliding introduces significant additional energy in the structure. As a result, the maximum intensity of excitation has a strong influence on the FPS design. In general, a FPS isolator designed for a particular level of excitation may not give satisfactory performance during an earthquake with much lower or higher intensity (Sinha and Pranesh, 1998). Due to the constant value of frequency, a resonant problem may occur when the structure resting on a FPS is subjected to a ground motion of dominant frequency close to the isolation frequency (Krishnamoorthy, 2010).

Due to the limitations of FPS, many researchers have tried different geometries for the sliding surface of the isolator. A recently developed new isolator, called as the variable frequency pendulum isolator (VFPI), incorporates the advantages of both FPS and PF isolators and overrules the disadvantages of FPS and PF isolators (Pranesh and Sinha, 1998; Pranesh, 2000). This is probably the first attempt to propose the concept of variable frequency in the sliding type isolators, although the concept of variable curvature is found in literature earlier (Sustov, 1992). Lu et al. (2006) generalized the mathematical formulation of a sliding surface with variable curvature by using a polynomial function to define the geometry of the sliding surface. In this paper an experimental and analytical study of the performance of three sliding-type isolators (including VFPI) is carried out. Krishnamoorthy (2010) also proposed a sliding surface with variable frequency and friction coefficient. This study proposed an isolator having the radius of curvature varying exponentially with sliding displacement and friction coefficient also varying with the sliding displacement. However, VFPI is found to be more effective under a variety of excitations and structures because of the following properties of VFPI: (1) its time period of oscillation depends on the sliding displacement, and (2) its restoring force has a bounded value and exhibits softening behaviour for the large displacements (Malu and Murnal, 2010). The geometry of sliding surface is defined by a second-order parametric equation. As a result, the isolator properties can be chosen to achieve the progressive period shift with a variation in the sliding displacement. These properties can be controlled by a set of VFPI parameters, which is otherwise not possible in the single-parameter systems like FPS.

The study of structures subjected to near-fault ground motions has a special significance due to the nature of such ground motions. The near-fault ground motions are characterized by pulse-type excitations having a narrow range of relatively lower frequencies. These motions often contain strong coherent dynamic long-period pulses and permanent ground displacements. The dynamic motions are dominated by the large long-period pulses of motions that are caused by the rupture directivity effects and occur on the horizontal component perpendicular to the strike of fault. This pulse is a narrow-band pulse which causes the response spectrum to have a peak, such that the response due to the near-fault ground motions of moderate magnitudes may exceed the response due to the near-fault ground motions of large magnitudes at intermediate periods. The radiation pattern of the shear dislocation on the fault causes this large pulse of motion to be oriented in the direction perpendicular to the fault plane, thus causing the strike-normal component of the ground motion to be larger than the strike-parallel component. The strike-parallel motion causes a permanent ground displacement (i.e., fling step), whereas the strike-normal component causes a significantly higher dynamic motion (Somerville, 1997, 2005).

The structures isolated by most base isolation devices have long time periods which are fairly constant. Since the near-fault ground motions are long-period, pulse-type motions, those induce very large displacements at the isolation level. As a result, base-isolated structures do not perform well under the near-fault ground motions. However, it has been demonstrated that the newly developed isolator VFPI can be effective under both near-fault and far-field ground motions, if proper VFPI parameters are adopted in the design (Murnal and Malu, 2007; Malu and Murnal, 2010). However, it is difficult to control the large sliding displacements that could occur during the near-fault ground motions.

In the present paper, it is proposed to change the coefficient of friction at a predefined location along the VFPI isolator surface so that the sliding displacement can be controlled under the near-field ground motions. A smaller value of the coefficient of friction for smaller sliding displacements and a larger value for larger sliding displacements is likely to control the displacement due to the higher energy dissipation due to the increased friction force. The effectiveness of a VFPI with discretely variable coefficient of friction is examined through a parametric study on the single-degree-of-freedom (SDOF) models (i.e., 2-DOF models when isolated) subjected to near-fault ground motions.

VFPI DESCRIPTION

1. Mathematical Preliminaries

Consider the motion of a rigid block of mass m sliding on a smooth curved surface of the defined geometry, $y = f(x)$. The restoring force offered by the curved sliding surface can be defined as the lateral force required to cause the horizontal displacement x. Assuming a point contact between the block and the sliding surface, various forces acting on the sliding surface, when the block is displaced from its original position at the origin of coordinate axes, are as shown in Figure 1. At any instant, the horizontal restoring force due to the weight of the structure is given by

$$f_R = mg \frac{\mathrm{d}y}{\mathrm{d}x} \tag{1}$$

Assuming that the restoring force is mathematically represented by an equivalent nonlinear massless horizontal spring, the spring force can be expressed as the product of the equivalent spring stiffness and deformation, i.e.,

$$f_R = k(x)x \tag{2}$$

where $k(x)$ is the instantaneous spring stiffness, and x is the sliding displacement of the mass.

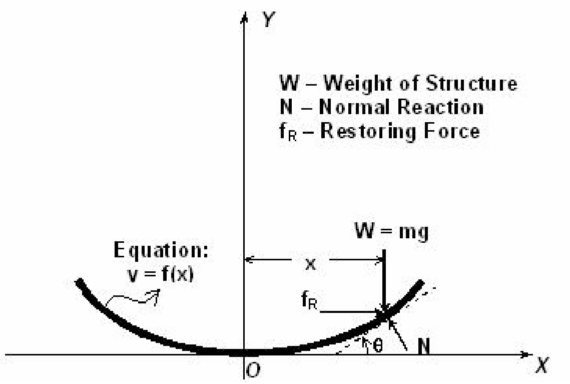

Fig. 1 Free-body diagram of sliding surface

If the mass is modelled as a single-degree-of-freedom oscillator, the spring force (or restoring force) can be expressed as the product of the total mass of the system and square of oscillation frequency:

$$f_R = m\omega_b^2(x)x \tag{3}$$

Here, $\omega_b(x)$ is the instantaneous isolator frequency; this depends solely on the geometry of the sliding surface. In a friction pendulum system, which has a spherical sliding surface, this frequency is almost constant and is approximately equal to $\sqrt{g/R}$, where R is the radius of curvature of the sliding surface (Zayas et al., 1990).

2. Variable Frequency Pendulum Isolator Geometry

A sliding surface based on the expression of an ellipse has been used as the basis for developing the sliding surface of VFPI (Pranesh, 2000). The equation of an ellipse with a and b as its semi-major and semi-minor axes, respectively, and with the coordinate axes as shown in Figure 1 is given by

$$y = b\left(1 - \sqrt{1 - x^2/a^2}\right) \tag{4}$$

On differentiating with respect to x, the slope at any point on the curve is given by

$$\frac{\mathrm{d}y}{\mathrm{d}x} = \frac{b}{a^2\sqrt{1 - x^2/a^2}}x \tag{5}$$

If the equation of sliding surface is represented by Equation (4), the frequency of oscillation can be determined by substituting Equation (5) in Equations (1) and (3). As a result, the expression for the frequency of elliptical surface is given by

$$\omega_b^2(x) = \omega_I^2 \Big/ \sqrt{1 - x^2/a^2} \tag{6}$$

where $\omega_I^2 = gb/a^2$ is the square of the initial frequency of the isolator (at the zero sliding displacement).

It can be seen that the frequency of an elliptical curve is fairly constant for small displacements (i.e., $x << a$) and that this value depends on the ratio, b/a^2. From this expression, it is observed that the frequency of the surface is inversely proportional to the square of semi-major axis and that an increase in its value results in a sharp decrease in the isolator frequency. Hence, in order to get the desired variation in the isolator frequency, the semi-major axis of the ellipse, a, is taken as a linear function of the sliding displacement x and is expressed as a variable in getting the geometry of VFPI. The semi-major axis can thus be expressed as

$$a = x + d \tag{7}$$

where d is a constant. On substituting Equation (7) in Equation (4), the expression for the geometry of the sliding surface of VFPI becomes

$$y = b\left[1 - \frac{\sqrt{d^2 + 2dx\,\mathrm{sgn}(x)}}{d + x\,\mathrm{sgn}(x)}\right] \tag{8}$$

where $\mathrm{sgn}(x)$ is the signum function introduced for maintaining the symmetry of sliding surface about the central vertical axis. This function assumes a value of +1 for the positive sliding displacements and −1 for the negative sliding displacements. It is observed from Equation (8) that the upper bound of vertical displacements is equal to b and that this occurs only at infinitely large horizontal displacements. The slope at any point on this sliding surface is given as

$$\frac{\mathrm{d}y}{\mathrm{d}x} = \frac{bd}{\left(d + x\,\mathrm{sgn}(x)\right)^2 \sqrt{d^2 + 2dx\,\mathrm{sgn}(x)}}\,x \tag{9}$$

To simplify the notations, a non-dimensional parameter $r = x\,\mathrm{sgn}(x)/d$ is used. On substituting r and the initial frequency squared $\omega_I^2 = gb/d^2$ in Equation (9) and on combining with Equations (1) and (2), the square of the isolator frequency at any sliding displacement can be expressed as

$$\omega_b^2(x) = \frac{\omega_I^2}{(1+r)^2\sqrt{1+2r}} \tag{10}$$

In the above equations, the parameters b and d completely define the isolator characteristics. It can also be observed that the ratio, b/d^2, governs the initial frequency of the isolator. Similarly, the value of $1/d$ determines the rate of variation of the isolator frequency. Let this factor be defined as the frequency variation factor (FVF). It is also seen from Equation (10) that the rate of decrease in the isolator frequency is directly proportional to FVF for a given initial frequency. The variation in the oscillation frequency of a typical VFPI with respect to sliding displacement is shown in Figure 2(a). For the purpose of comparison, the oscillation frequency of FPS with the same initial frequency is also shown and is found to be almost constant. From this plot, it is seen that the oscillation frequency of VFPI sharply decreases with the increasing sliding displacement and asymptotically approaches zero. The force-deformation hysteresis curves obtained from Equation (3), for a typical FPS and VFPI, are shown in Figure 2(b). In this plot, the isolator force (i.e., restoring force plus frictional force) is normalized with respect to mg and both constant and discretely variable coefficients of friction are considered. It can be observed that the isolator force in VFPI first increases to reach its maximum value and later decreases slowly so as to asymptotically approach the frictional force at large sliding displacements for a constant coefficient of friction. This is an important property of VFPI, which limits the force transmitted to the structure. Beyond the peak restoring force, the VFPI does not lose the restoring capability since a small amount of restoring force is always available. It is also observed that for very small displacements, the variation in restoring force is approximately linear. In the FPS, on the other hand, the restoring force always increases linearly with the sliding displacement. From this, it can be concluded that the behaviour of VFPI is similar to that of FPS for small displacements and similar to that of PF for large displacements without a significant loss of restoring capability. In the case of a variable coefficient of friction, the isolator force suddenly changes at a point where the coefficient of friction undergoes a change in its value, while the rest of the variation remains unchanged. This will change the energy dissipation characteristics of the isolator which may help in controlling the sliding displacements.

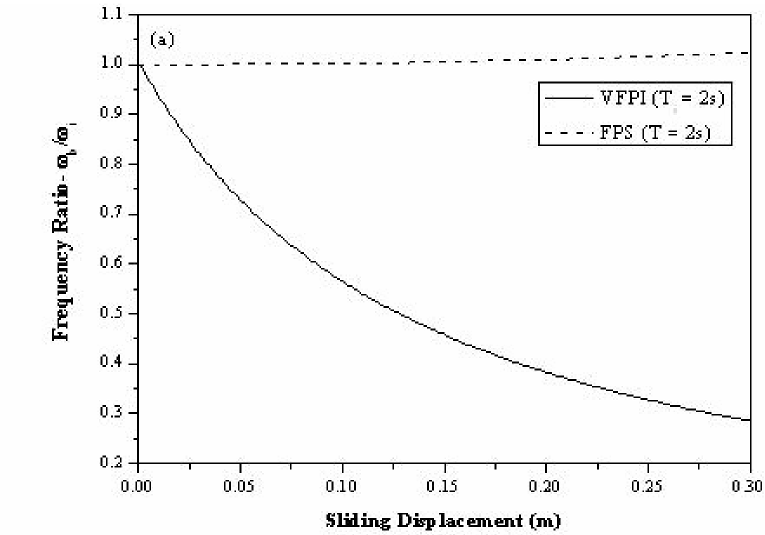

(a)

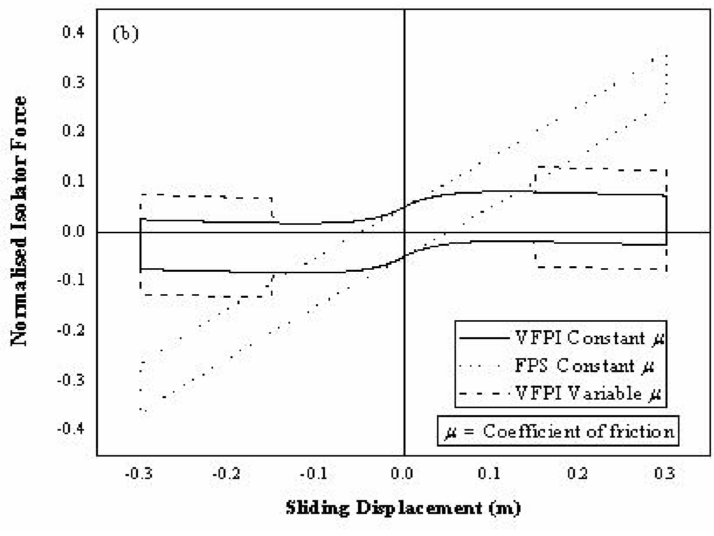

(b)

Fig. 2 Comparison of variations of (a) frequency ratio and (b) normalized isolator force with sliding displacement for VFPI and FPS (with $\mu = 0.05$, $\mu_1 = 0.05$ and $\mu_2 = 0.1$)

The geometries of the sliding surfaces of VFPI and FPS are shown in Figure 3. From this figure, it can be easily observed that a VFPI is flatter than a FPS, which results in smaller vertical displacements for similar sliding displacements in the structure and hence may lead to smaller overturning moments.

MATHEMATICAL FORMULATION

Consider a single-storey shear structure isolated by a sliding type isolator (i.e., a two-DOF system when isolated) when it is subjected to the horizontal ground excitation $\ddot{x}_g$ (see Figure 4). The forces acting on the isolator, when sliding is in the positive x-direction, are same as those shown in Figure 1.

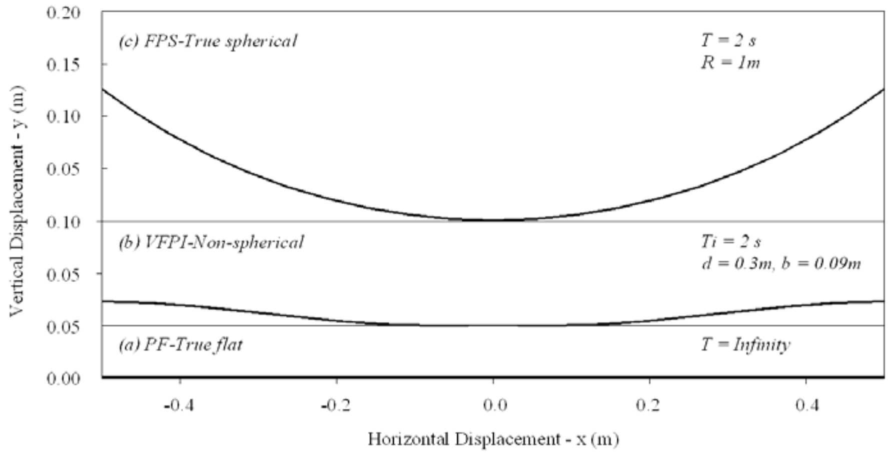

Fig. 3 Geometries of sliding surfaces of PF, VFPI and FPS isolators

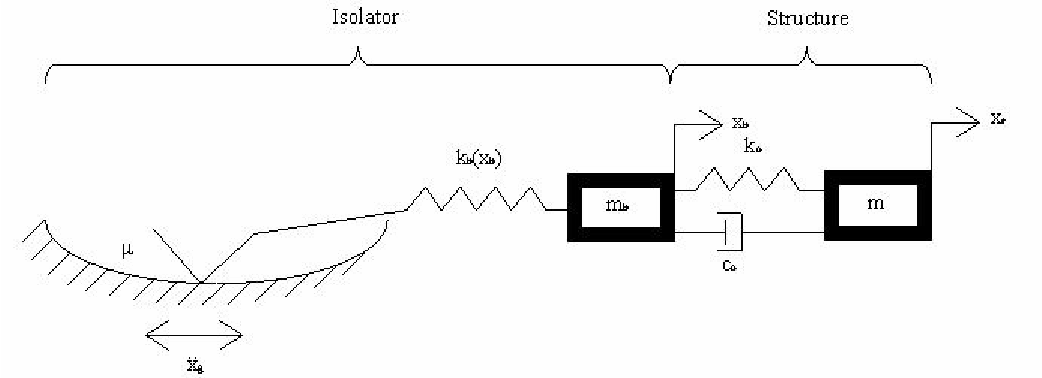

Fig. 4 Analytical model of single-storey structure isolated by curved sliding surface

1. Equations of Motion

The motion of structure can be in either of the two phases: non-sliding phase and sliding phase. In the non-sliding phase, the structure behaves like a conventional fixed-base structure, since there is no relative motion at the isolator level. When the frictional force at the sliding surface is overcome, there is a relative motion at the sliding surface and the structure enters the sliding phase. The total motion consists of a series of alternating non-sliding and sliding phases in succession.

2. Non-sliding Phase

In the non-sliding phase, the structure behaves as a fixed-base structure. There is no relative motion between the ground and base mass, since the static frictional resistance is greater than the horizontal force acting on the structure. The equations of motion in this phase are

$$\ddot{x}_r + 2\xi_o\omega_o\dot{x}_r + \omega_o^2 x_r = -\ddot{x}_g \tag{11}$$

and

$$x_b = \text{constant};\ \dot{x}_b = \ddot{x}_b = 0 \tag{12}$$

where x_r is the relative displacement of the top mass with respect to the base mass, x_b is the displacement of the base mass m_b relative to the ground, and x_g is the ground displacement. Further, an overdot indicates a derivative with respect to time, and $\omega_o = \sqrt{k_o/m}$ and $\xi_o = c_o/2\sqrt{k_o m}$ are the frequency and damping ratio, respectively, of the fixed-base SDOF structure. Before the application of ground motion, the structure is at rest; as a result, the motion of structure always starts in the non-sliding phase. The structure is classically damped in this phase and hence the equation of motion can be readily solved by the usual modal analysis procedures (Clough and Penzien, 1993).

3. Initiation of Sliding Phase

When the structure is subjected to a base excitation, it will remain in the non-sliding phase unless the frictional resistance at the sliding surface is overcome. This means that the absolute value of the sum of the total inertia force and restoring force should be greater than or equal to the absolute value of the frictional force acting along the sliding surface. The frictional force depends on the coefficient of friction at the location at a given instant. The plan of a typical isolator with two discrete values of the coefficient of friction considered in this study is shown in Figure 5. The coefficient of friction, μ_1, is assumed to be less than μ_2 in this study. Therefore, the condition for the beginning of the sliding phase can be written as

$$\left|\left[m\left(\ddot{x}_r+\ddot{x}_g\right)+m_b\ddot{x}_g\right]\cos\theta+\left(m+m_b\right)g\sin\theta\right|\geq\mu\left(m+m_b\right)g\cos\theta \tag{13}$$

where θ is the angle of tangent at the point of contact with horizontal and μ (= μ_1 or μ_2) is the coefficient of friction at the respective isolator positions. Now, on dividing Equation (13) by $\cos\theta$ and substituting $\mathrm{d}y/\mathrm{d}x_b$ for $\tan\theta$, the condition for sliding can be simplified as

$$\left|\left[m\left(\ddot{x}_r+\ddot{x}_g\right)+m_b\ddot{x}_g\right]+\left(m+m_b\right)g\frac{\mathrm{d}y}{\mathrm{d}x_b}\right|\geq\mu\left(m+m_b\right)g\,;\ \mu=\mu_1\text{ or }\mu_2 \tag{14}$$

Here, $\left(m+m_b\right)g\,\mathrm{d}y/\mathrm{d}x_b$ is the restoring force (see Equation (1)). If this is expressed as a product of the spring stiffness and sliding displacement, the spring force is given by (see Equation (3))

$$f_R=\left(m+m_b\right)\omega_b^2\left(x_b\right)x_b \tag{15}$$

where $\omega_b\left(x_b\right)$ is the isolator frequency at the instant for the sliding displacement x_b. On dividing Equation (14) by the total mass and on defining the mass ratio as

$$\alpha=\frac{m}{m+m_b} \tag{16}$$

the condition for the initiation of the sliding phase can be simply expressed as

$$\left|\alpha\ddot{x}_r+\ddot{x}_g+\omega_b^2\left(x_b\right)x_b\right|\geq\mu g\,;\ \mu=\mu_1\text{ or }\mu_2 \tag{17}$$

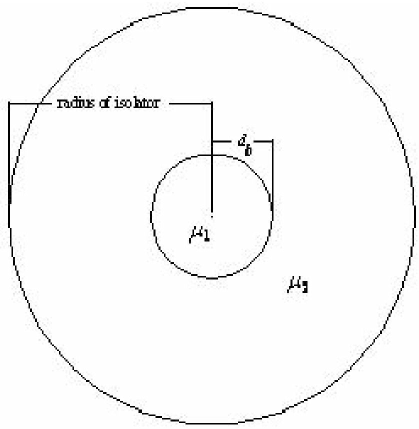

Fig. 5 Plan of typical isolator with variable coefficient of friction

4. Sliding Phase

Once the inequality (see Equation (14)) is satisfied, the static frictional force is overcome, the structure enters the sliding phase, and the degree of freedom (DOF) corresponding to the base mass also experiences motion. During this phase, the structure behaves like a two-degree-of-freedom structure. The equations of motion for the top and bottom masses are respectively given by

$$\ddot{x}_r+2\xi_o\omega_o\dot{x}_r+\omega_o^2x_r=-\ddot{x}_b-\ddot{x}_g \tag{18}$$

and

$$\alpha \ddot{x}_r + \ddot{x}_b + \omega_b^2(x_b)x_b = -\ddot{x}_g - \mu g \,\mathrm{sgn}(\dot{x}_b);\ \mu = \mu_1 \text{ or } \mu_2 \tag{19}$$

5. End of Sliding Phase

The sliding phase ends when the sliding velocity of the base mass becomes equal to zero, i.e.,

$$\dot{x}_b = 0 \tag{20}$$

As soon as this condition is satisfied, Equations (11) and (12) corresponding to the non-sliding phase need to be evaluated to further check the validity of the inequality in Equation (17). This decides whether the structure continues in the sliding phase after a momentary stop or enters the non-sliding phase.

6. Direction of Sliding

Once the inequality (see Equation (17)) is satisfied, the structure starts sliding in a direction opposite to the direction of the sum of the total inertia force and restoring force at the isolator level. Thus, the direction of sliding can be decided based on the signum function as defined below:

$$\mathrm{sgn}(\dot{x}_b) = -\frac{\alpha \dot{x}_r + \ddot{x}_g + \omega_b^2(x_b)}{\left|\alpha \dot{x}_r + \ddot{x}_g + \omega_b^2(x_b)\right|} \tag{21}$$

The signum function remains unchanged in a particular sliding phase until the sliding velocity of the base mass becomes equal to zero. Once the sliding velocity is zero, the structure may enter the non-sliding phase, reverse its direction of sliding, or have a momentary stop and then continue in the same direction. To determine the correct state, the solution process needs to continue while using the equations of non-sliding phase wherein the sliding acceleration is forced to be zero and the validity of the inequality (see Equation (17)) is checked. If this inequality is satisfied at the same instant of time when the sliding velocity is zero, Equation (21) decides the further direction of sliding.

RESPONSE OF AN EXAMPLE SYSTEM

The effectiveness of VFPI with a variable coefficient of friction to reduce the response of an example single-storey structure subjected to the near-fault earthquake excitations is presented in this section. The example structure, under the fixed-base condition, is represented as an SDOF system, with the values of spring stiffness and lumped mass taken such that the period of the structure is 0.5 s. The masses of the structure and base are taken equal, such that the mass ratio α becomes 0.5.

Narasimhan and Nagarajaiah (2006) proposed a variable-friction system to adjust the level of friction in the base-isolated structures. Panchal and Jangid (2008) proposed a sliding surface by varying the friction coefficient along the sliding surface in the form of the curve of FPS and called the isolator as VFPS. In this case, the value of the coefficient of friction changes from a minimum of 0.025 to a maximum of 0.15 and then again reduces and approaches ~0.015. Krishnamoorthy (2010) proposed a variable frequency and variable friction pendulum isolator (VFFPI). Here, the value of the coefficient of friction changes from a minimum of 0.08 to a maximum of 0.1 in between the distance of 0.0 to 0.18 m from the centre of the sliding surface. These studies show that a sliding isolator with either a varying radius of curvature or a varying friction coefficient may be used as an effective isolator for isolating the structure. Most of these studies have focussed on the effectiveness of the isolator in reducing accelerations under different excitations. However, all of these isolators are likely to be of limited effectiveness under the near-fault ground motions due to very high sliding displacements. Further, it may be practically difficult to achieve a sliding surface with a continuously variable coefficient of friction of desired variation. Hence, in the present study, the performance of VFPI with two discrete values of the coefficient of friction, i.e., the initial coefficient of friction, μ_1, and the final coefficient of friction, μ_2, under the near-fault ground motions is evaluated.

The behaviour of VFPI is studied through a time-history analysis for ten near-fault ground motion records. The details of the ground-motion records used in the study are presented in Table 1. These ground-motion records are derived from the actually recorded motions. The ground motions chosen cover a wide variety of near-fault ground motions having different peak ground acceleration (PGA) values, frequency compositions and durations. For a given coefficient of friction, the main parameters of VFPI affecting the response are (i) initial time period and (ii) frequency variation factor (FVF). For the present analysis, FVF is varied from 1.0 per m to 10.0 per m for a VFPI with two values of initial time period, 1 and 2 s. In order to investigate the effectiveness of VFPI, the responses are compared with those of the structure isolated by using a FPS with the isolator period equal to 2.0 s, which is a practical value for such a system.

Table 1: Details of Ground-Motion Records Used in This Study

S. No.	Name of Earthquake	Designation	Magnitude	Distance of Source (km)	PGA (g)	Duration (s)
1	1978 Tabas	NFR-01	7.4	1.2	0.900	50
2	1989 Loma Prieta	NFR-02	7.0	3.5	0.718	25
3	1989 Loma Prieta	NFR-03	7.0	6.3	0.686	40
4	1992 Cape Mendocino	NFR-04	7.1	8.5	0.638	60
5	1992 Erzincan	NFR-05	6.7	2.0	0.432	21
6	1992 Landers	NFR-06	7.3	1.1	0.713	50
7	1994 Nothridge	NFR-07	6.7	7.5	0.890	15
8	1994 Nothridge	NFR-08	6.7	6.4	0.732	60
9	1995 Kobe	NFR-09	6.9	3.4	1.088	60
10	1995 Kobe	NFR-10	6.9	4.3	0.786	40

In order to study the effect of variable coefficient of friction on the behaviour of a VFPI-isolated structure, two values of the coefficient of friction considered are $\mu_1 = 0.05$ and $\mu_2 = 0.1$. The VFPIs with these two constant coefficients of friction are first analyzed separately and then they are combined in the same isolator, the latter case being referred to as the case of variable coefficient of friction. In this case the initial coefficient of friction, μ_1, refers to the coefficient of friction up to a pre-defined distance d_b from the centre of the isolator, and the coefficient of friction beyond this distance is referred to as the final coefficient of friction, μ_2. The values $\mu_1 = 0.05$ and $\mu_2 = 0.1$ considered in this study should enable a larger energy dissipation for a larger sliding displacement, which may help to control the sliding displacements. For the change of coefficient of friction, three positions are considered from the centre of the isolator: $d_b = 0.1$, 0.3 and 0.5 m. The structural damping is assumed as 5% of critical.

1. Time-History Response

The response quantities are evaluated by the solution of the equations of motion as discussed in the preceding sections. The main response quantities of interest are the absolute acceleration of the top storey and the sliding displacement of the isolator. To show the effectiveness of VFPI with respect to FPS, typical time-history graphs for NFR-01 (i.e., the normal component of the 1978 Tabas earthquake motion) are shown in Figures 6 and 7. Figure 6 shows the acceleration time histories for VFPI and FPS with the constant coefficient of friction of 0.05. As expected, it is seen that the accelerations are substantially reduced in the case of VFPI as compared to FPS.

It is expected that varying the coefficient of friction along the sliding surface will lead to a decrease in the sliding displacement. This is usually a matter of concern for the VFPIs, especially under the near-field ground motions. To show the effectiveness of the variable coefficient of friction, typical time-history graphs of sliding displacement under NFR-01 are shown in Figure 7. This figure shows the time-histories of sliding displacement for the cases of constant coefficient of friction and variable coefficient of friction under the three different values of d_b. It is seen that the sliding displacements are effectively controlled in the case of variable coefficient of friction and that this case is more effective for the lesser values of

d_b. This implies that it is possible to control the sliding displacements by using a variable coefficient of friction under the near-field ground motions without any significant increase in the accelerations.

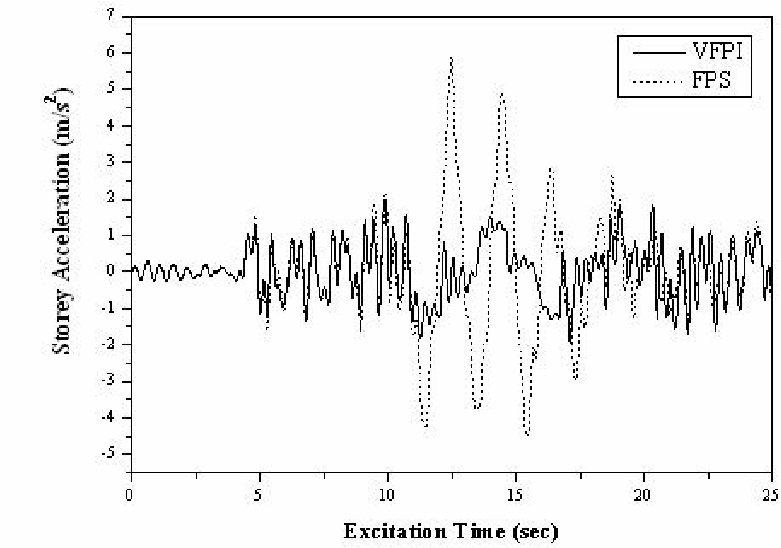

Fig. 6 Comparison of time-history curves of storey acceleration for VFPI and FPS with constant coefficient of friction (for NFR-01, FVF = 2 and $\mu = 0.05$)

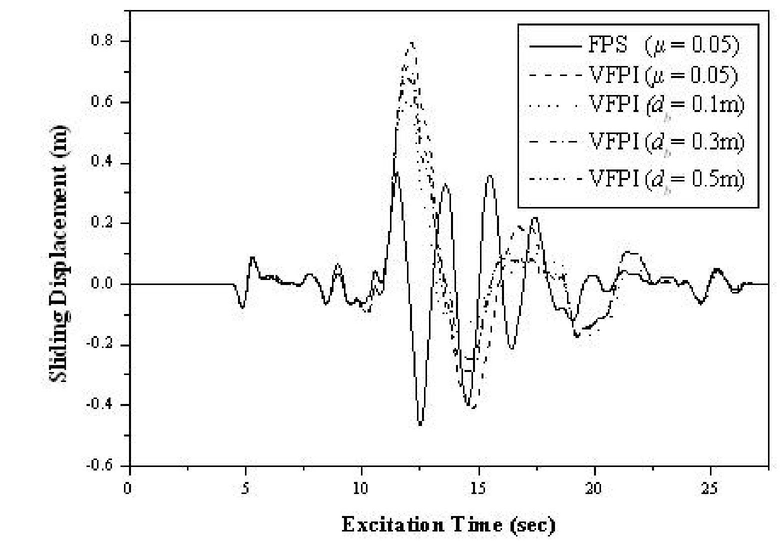

Fig. 7 Comparison of time-history curves of sliding displacement for VFPI and FPS with constant and variable coefficients of friction (for NFR-01, FVF = 2, $\mu = 0.05$, $\mu_1 = 0.05$ and $\mu_2 = 0.1$)

To further ascertain the effectiveness of variable coefficient of friction in reducing the sliding displacements, a comparison of the force-deformation histories for constant and variable coefficients of friction in the VFPI of T_i = 2 s is presented in Figure 8 for the case of NFR-01, FVF = 2 and d_b = 0.1 m. From this figure, it is clear that sliding displacements are controlled in the case of variable coefficient of friction due to higher energy dissipation in this case, since the area under the force-deformation graph increases due to the increased coefficient of friction at the predefined point.

2. Effect of Variable Coefficient of Friction

Under the near-fault excitations, a FPS may be able to control the sliding displacements, but it may also lead to very high levels of structural accelerations due to the long-period pulse-type components in the excitation. On the other hand, a VFPI can control the accelerations but at the cost of high sliding displacements. Hence, a VFPI with variable coefficient of friction is likely to control both accelerations and sliding displacements. Varying the coefficient of friction may not help in the case of FPS as the displacements are already controlled with a constant coefficient of friction and accelerations are bound to be high in any case due to the constant time period of FPS. In order to present the responses with effective comparison and comprehension, the maximum response quantities of the structures isolated with a VFPI are normalized with respect to the corresponding response quantity, with the FPS having a constant time period of 2.0 s and the corresponding value of the coefficient of friction. For example, the maximum response values with the VFPI of μ = 0.05 are normalized with respect to the maximum response value with the FPS of μ = 0.05, and the maximum response values with the VFPI of μ = 0.1 are normalized with respect to the maximum response value with the FPS of μ = 0.1. In the case of variable coefficient of friction, the response quantities are normalized with the FPS having a constant coefficient of friction of 0.05, since varying the coefficient of friction in the case of FPS will not add to any advantage in the performance. This means that the maximum response values with a VFPI of variable coefficient of friction are normalized with respect to the maximum response value with the FPS of μ = 0.05. Thus, the isolation is more effective when the normalized accelerations are less than unity (i.e., less than the corresponding response with the FPS) and the normalized sliding displacements are marginally greater than unity (which is the displacement control equivalent to the FPS).

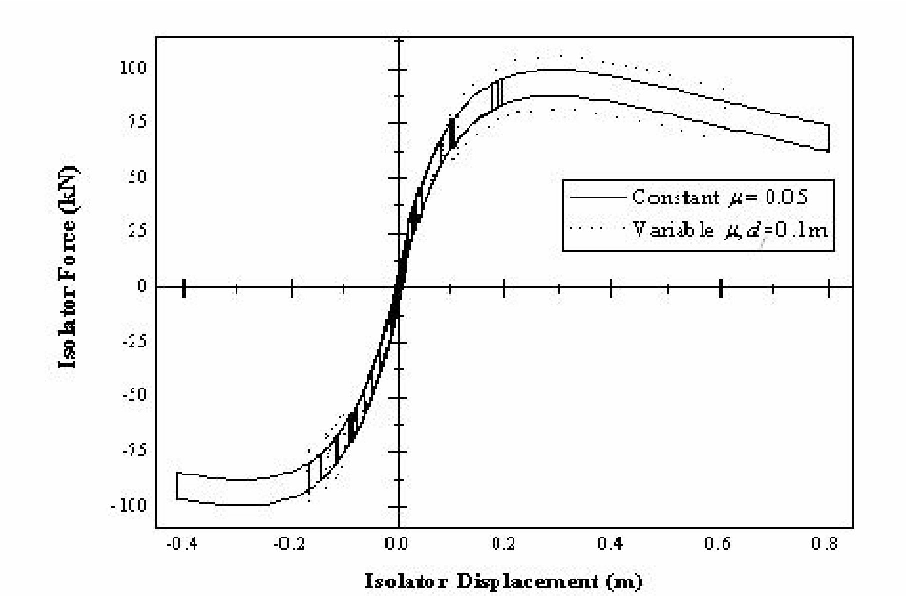

Fig. 8 Comparison of force-deformation histories of VFPI for constant and variable coefficients of friction (for NFR-01, FVF = 2, $\mu = 0.05$, $\mu_1 = 0.05$, $\mu_2 = 0.1$ and d_b = 0.1 m)

For different cases under consideration, time-history analyses are carried out for all the ten near-fault ground motions described in Table 1. Since these ground motions cover a wide variety of near-fault ground motions, the average of the maximum responses under the ten ground motions is considered for discussion. This is normalized by the average response of the corresponding FPS-isolated structures as explained earlier. The averages of maximum storey acceleration and sliding displacement responses with the FPS, using which the averages of maximum responses with the VFPI are normalized, are given in Table 2 for μ = 0.05 and 0.1. The normalized storey accelerations with the VFPIs for two constant and three variable coefficients of friction cases are compared in Figures 9 and 10 respectively for T_i = 1 and 2 s. Similarly, the normalized average sliding displacements with the VFPIs for two constant and three variable coefficients of friction cases are compared in Figures 11 and 12 respectively for T_i = 1 and 2 s.

From Figures 9 and 10, as expected, it is observed that the accelerations in the VFPI-isolated system are substantially reduced when compared to those in the FPS-isolated system, in all the cases. When the initial time period of VFPI is 1.0 s, it is observed that the accelerations sharply decrease with FVF (because of the sharp decrease in the restoring force), whereas there is no significant decrease in the accelerations with FVF in the case of VFPI with the initial time period of 2.0 s. Further, as expected, the accelerations under a lower coefficient of friction of 0.05 are substantially lower than those with a higher coefficient of friction of 0.1. The same observation also holds true in the cases of variable coefficient of friction, and the accelerations in all such cases (with different values of d_b) fall in between the accelerations for the two cases of constant coefficient of friction. However, those are closer to the lower bound of accelerations (i.e., for the case of the coefficient of friction of 0.05), which shows the effectiveness of a variable coefficient of friction in acceleration reduction.

Table 2: Average Peak Response Values for FPS-Isolated Structure with T = 2 s

S. No.	Description of Response	Unit	Peak Response Values for Coefficient of Friction	
			0.05	0.1
1	Storey acceleration	m/s^2	12.915	8.140
2	Sliding displacement	m	0.614	0.490

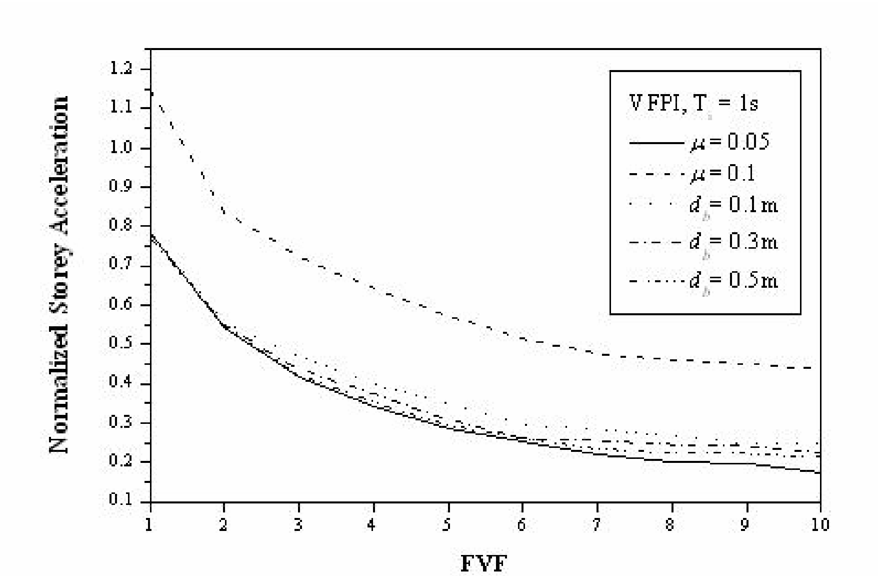

Fig. 9 Comparison of storey accelerations with different cases of VFPIs (of T_i = 1 s) as normalized with respect to peak values with FPS as in Table 2

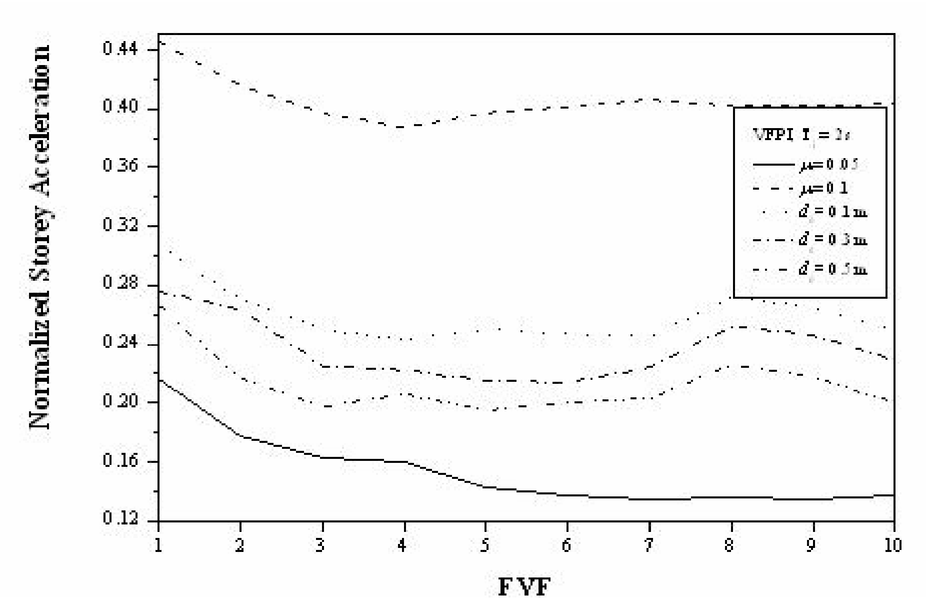

Fig. 10 Comparison of storey accelerations with different cases of VFPIs (of T_i = 2 s) as normalized with respect to peak values with FPS as in Table 2

From Figures 11 and 12, it is observed that the normalized sliding displacements increase with an increase in FVF in all the cases, since the increase in FVF leads to a reduction in the restoring force. As expected, the displacements for the lower coefficient of friction are higher than those for the higher coefficient of friction. It is interesting to note that the sliding displacements in some cases of variable coefficient of friction (see, for example, the results for d_b = 0.1 m) are lower than those in both the cases of constant coefficient of friction. It is also seen that sliding displacements are significantly lower for a FVF of 4–6 for the VFPI with the initial time period of 1.0 s and for a FVF of 1 to 3 for the VFPI with the initial time period of 2.0 s. It can be further confirmed that for this range of FVF, the accelerations are also significantly lower (around 20% to 30% of those in the case of FPS). Thus, it can be concluded that by varying the coefficient of friction at a suitable location on the isolator surface and by selecting suitable FVF and initial time period, it is possible to control both accelerations and sliding displacements.

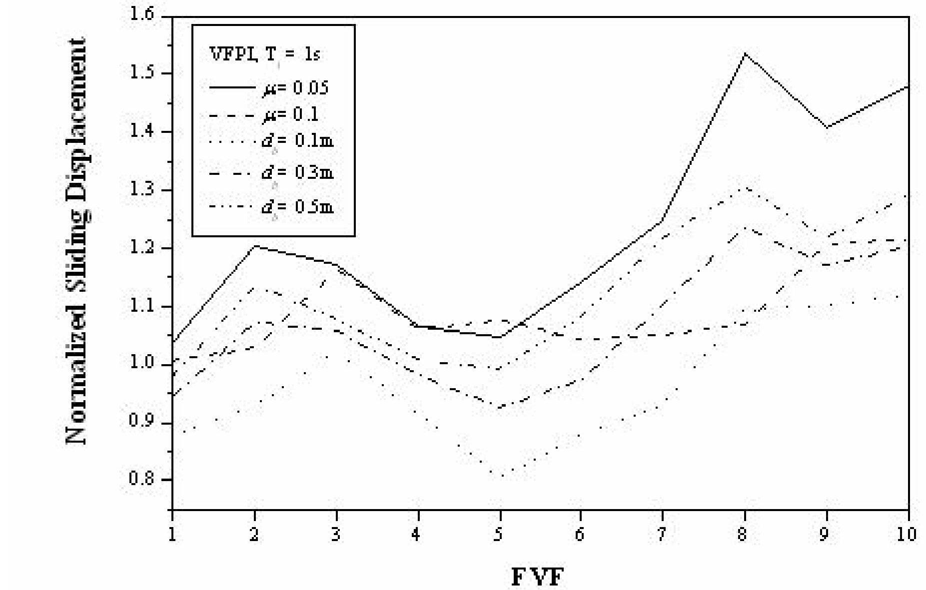

Fig. 11 Comparison of sliding displacements with different cases of VFPIs (of T_i = 1 s) as normalized with respect to peak values with FPS as in Table 2

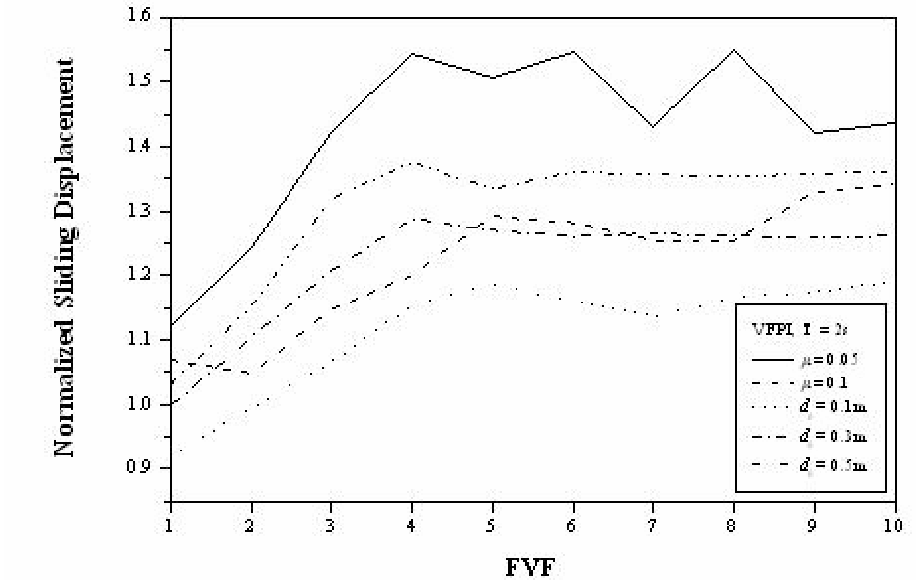

Fig. 12 Comparison of sliding displacements with different cases of VFPIs (of T_i = 2 s) as normalized with respect to peak values with FPS as in Table 2

CONCLUSIONS

The effectiveness of a recently developed isolation system, the variable frequency pendulum isolator (VFPI), for the vibration control of a single-storey structure subjected to the near-fault ground motions has been investigated in this paper. For the effectiveness of a VFPI in controlling both accelerations and sliding displacements under the near-field ground motions, a variable coefficient of friction for the sliding surface has been proposed in this paper. Based on the investigations, the following conclusions can be drawn:

1. A VFPI has a wide choice of parameters that can be chosen to suit the design requirements.
2. A VFPI is very effective for acceleration reduction under the action of near-fault ground motions, with a corresponding increase in the sliding displacements.
3. It is possible to control both accelerations and sliding displacements by using a variable coefficient of friction and by carefully choosing the VFPI parameters.

REFERENCES

1. Buckle, I.G. and Mayes, R.L. (1990). "Seismic Isolation: History, Application, and Performance—A World View", Earthquake Spectra, Vol. 6, No. 2, pp. 161–201.
2. Clough, R.W. and Penzien, J. (1993). "Dynamics of Structures", McGraw-Hill, New York, U.S.A.
3. Kelly, J.M. (1993). "State-of-the-Art and State-of-the-Practice in Base Isolation", Proceedings of ATC-17-1 Seminar on Seismic Isolation, Passive Energy Dissipation, and Active Control, San Francisco, U.S.A., Vol. 1, pp. 9–28.
4. Krishnamoorthy, A. (2010). "Seismic Isolation of Bridges Using Variable Frequency and Variable Friction Pendulum Isolator System", Structural Engineering International, Vol. 20, No. 2, pp. 178–184.
5. Lu, L.-Y., Wang, J. and Hsu, C.-C. (2006). "Sliding Isolation Using Variable Frequency Bearings for Near-Fault Ground Motions", Proceedings of the 4th International Conference on Earthquake Engineering, Taipei, Taiwan, Paper No. 164 (on CD).
6. Malu, G. and Murnal, P. (2010). "Behavior of Structure with VFPI during Near-Field Ground Motion", Proceedings of International Conference on Innovative World of Structural Engineering (ICIWSE-2010), Aurangabad, Vol. I, pp. 166–174.
7. Mokha, A., Constantinou, M. and Reinhorn, A. (1990). "Teflon Bearings in Base Isolation. I: Testing", Journal of Structural Engineering, ASCE, Vol. 116, No. 2, pp. 438–454.
8. Mostaghel, N., Hejazi, M. and Tanbakuchi, J. (1983). "Response of Sliding Structures to Harmonic Support Motion", Earthquake Engineering & Structural Dynamics, Vol. 11, No. 3, pp. 355–366.
9. Murnal, P. and Malu, G.M. (2007). "Selection of VFPI Parameters for Isolation Effectiveness during Near-Field Ground Motion", Proceedings of the 8th Pacific Conference on Earthquake Engineering, Singapore, Paper No. 105 (on CD).
10. Naeim, F. and Kelly, J.M. (1999). "Design of Seismic Isolated Structures: From Theory to Practice", John Wiley, New York, U.S.A.
11. Narasimhan, S. and Nagarajaiah, S. (2006). "Smart Base Isolated Buildings with Variable Friction Systems: H_∞ Controller and SAIVF Device", Earthquake Engineering & Structural Dynamics, Vol. 35, No. 8, pp. 921–942.
12. Panchal, V.R. and Jangid, R.S. (2008). "Variable Friction Pendulum System for Seismic Isolation of Liquid Storage Tanks", Nuclear Engineering and Design, Vol. 238, No. 6, pp. 1304–1315.
13. Pranesh, M. (2000). "VFPI: An Innovative Device for Aseismic Design", Ph.D. Thesis, Indian Institute of Technology Bombay, Mumbai.
14. Pranesh, M. and Sinha, R. (1998). "Vibration Control of Primary-Secondary Systems Using Variable Frequency Pendulum Isolator", Proceedings of the Eleventh Symposium on Earthquake Engineering, Roorkee, Vol. II, pp. 697–704.
15. Shustov, V. (1992). "Base Isolation: Fresh Insight", Proceedings of the Tenth World Conference on Earthquake Engineering, Madrid, Spain, Vol. 4, pp. 1983–1986.

16. Sinha, R. and Pranesh, M. (1998). "FPS Isolator for Structural Vibration Control", Proceedings of International Conference on Theoretical, Applied, Computational and Experimental Mechanics (ICTACEM98), Kharagpur (on CD).
17. Somerville, P. (1997). "Engineering Characteristics of Near Fault Ground Motion", Proceedings of SMIP97 Seminar on Utilization of Strong-Motion Data, Los Angeles, U.S.A., pp. 9–28.
18. Somerville, P.G. (2005). "Engineering Characterization of Near Fault Ground Motions", Proceedings of 2005 New Zealand Society for Earthquake Engineering Conference, Taupo, New Zealand, Paper No. 1 (on CD).
19. Tsai, C.S. (1997). "Finite Element Formulations for Friction Pendulum Seismic Isolation Bearings", International Journal for Numerical Methods in Engineering, Vol. 40, No. 1, pp. 29–49.
20. Tsopelas, P., Constantinou, M.C., Kim, Y.S. and Okamoto, S. (1996). "Experimental Study of FPS System in Bridge Seismic Isolation", Earthquake Engineering & Structural Dynamics, Vol. 25, No. 1, pp. 65–78.
21. Wang, Y.-P., Chung, L.-L. and Liao, W.-H. (1998). "Seismic Response Analysis of Bridges Isolated with Friction Pendulum Bearings", Earthquake Engineering & Structural Dynamics, Vol. 27, No. 10, pp. 1069–1093.
22. Zayas, V.A., Low, S.S. and Mahin, S.A. (1987). "The FPS Earthquake Resisting System: Experimental Report", Report UCB/EERC-87/01, University of California, Berkeley, U.S.A.
23. Zayas, V.A., Low, S.S. and Mahin, S.A. (1990). "A Simple Pendulum Technique for Achieving Seismic Isolation", Earthquake Spectra, Vol. 6, No. 2, pp. 317–333.

INSTRUCTIONS TO AUTHORS

1. Research papers, technical notes, state-of-the-art papers and reports on damaging earthquakes which have not been previously published or offered for publication elsewhere are considered for publication in the ISET Journal of Earthquake Technology. Discussions on any paper previously published in the Journal are also considered for publication. Articles submitted to the Journal should be original and should not be under consideration for publication elsewhere at the same time.

2. The PDF file of the manuscript should be submitted to the Editor electronically at ***vinaykg@iitk.ac.in*** for possible publication of an article in the Journal. The submission may alternatively be made to an Associate Editor: at ***manohar@civil.iisc.ernet.in*** for papers related to *Structural Dynamics*; at ***ramana@civil.iitd.ernet.in*** for *Soil Dynamics,* and ***mukutfeq@iitr.ernet.in*** for *Seismology and Seismotectonics*.

3. Following are specific requirements with regard to articles and formats:

   i. Paper length: The length of a paper should be restricted to 10000 words maximum

   ii. Headings and subheadings: Headings should be in bold uppercase and not numbered. Sub-headings should be in bold lower case and may be numbered.

   iii. Figures and Tables: These should be numbered consecutively in Arabic numerals and should be titled. Figure captions should be given on a separate sheet.

   iv. Photographs, illustrations: Good glossy bromide prints of these must accompany the manuscript and not be attached to the manuscript pages.

   v. References: These should be listed alphabetically at the end of the text and numbered serially. These should be cited in the text by the last name(s) of authors followed by the year of publication in parenthesis. In case of more than two authors, the last name of the first author followed by et al. and the year of publication is to be cited in the text. References are to be listed in the following format only:

   1. Krishna, J. and Chandrasekaran, A.R. (1964). "Earthquake Resistant Design of an Elevated Water Tower", Bull. Indian Soc. of Earthquake Tech., Vol. 1, No. 1, pp. 20-36.
   2. Prakash, S. (1960). "Soil Dynamics", McGraw Hill Book Co., New Delhi.
   3. Wason, H.R., Sharma, M.L., Pal, K. and Srivastava, L.S. (1986). "Digital Telemetered Seismic Array in Ganga-Yamuna Valley", Proc. 8th Symposium on Earthquake Engg., Roorkee, Vol. 2, pp. 91-99.
   4. Rai, D.C., Narayan, J.P., Pankaj and Kumar, A. (1997). "Jabalpur Earthquake of May 22, 1997: Reconnaissance Report", Deptt. of Earthquake Engineering, University of Roorkee, Roorkee.

   vi. Abstract: This should not exceed 150 words and be an abbreviated, accurate representation of the contents of the article. It should be followed by a list of 3 to 5 key words of these contents.

   vii. Units: All quantities should be in SI units. Other units may be enclosed in parentheses after the SI units, if necessary.

4. **Preparation for Publication:** Once accepted for publication, the final version of the article will be sent to the author(s) for proof checking. The author(s) should ensure that it is complete with no grammatical or spelling errors and return the same to the Co-Editor within 15 days.

ISSN 0972-0405

ISET JOURNAL OF EARTHQUAKE TECHNOLOGY

Vol. 49 No. 3-4 September-December 2012

CONTENTS

Financial Assistance from DST, New Delhi for the Publication of ISET Journals for 2012–2013 is duly acknowledged.

Published by : Dr. Ajay Chourasia, Co-Editor (2011-2013), Indian Society of Earthquake Technology, Roorkee
Printed at : R.K. Printers, RKE # Ph. : 01332-270957, 9897276995 E-mail : rkprint270957@gmail.com